Integrated Ocean Drilling Program
Expedition 304 Preliminary Report

Oceanic Core Complex Formation, Atlantis Massif

Oceanic core complex formation, Atlantis Massif, Mid-Atlantic Ridge: drilling into the footwall and hanging wall of a tectonic exposure of deep, young oceanic lithosphere to study deformation, alteration, and melt generation

17 November 2004–8 January 2005

Shipboard Scientific Party

PUBLISHER'S NOTES

Citation:
Expedition Scientific Party, 2005. Oceanic core complex formation, Atlantis Massif—oceanic core complex formation, Atlantis Massif, Mid-Atlantic Ridge: drilling into the footwall and hanging wall of a tectonic exposure of deep, young oceanic lithosphere to study deformation, alteration, and melt generation. *IODP Prel. Rept.,* 304. http://iodp.tamu.edu/publications/PR/304PR/304PR.PDF.

Distribution:
Electronic copies of this series may be obtained from the Integrated Ocean Drilling Program (IODP) Publication Services homepage on the World Wide Web at **iodp.tamu.edu/publications.**

This publication was prepared by the Integrated Ocean Drilling Program U.S. Implementing Organization (IODP-USIO): Joint Oceanographic Institutions, Inc., Lamont-Doherty Earth Observatory of Columbia University, and Texas A&M University, as an account of work performed under the international Integrated Ocean Drilling Program, which is managed by IODP Management International (IODP-MI), Inc. Funding for the program is provided by the following agencies:

European Consortium for Ocean Research Drilling (ECORD)

Ministry of Education, Culture, Sports, Science and Technology (MEXT) of Japan

Ministry of Science and Technology (MOST), People's Republic of China

U.S. National Science Foundation (NSF)

DISCLAIMER

April 2005

The following scientists and personnel were aboard the *JOIDES Resolution* for Expeditions 304 and 305 of the Integrated Ocean Drilling Program.

Expedition Scientific Party

Donna Blackman
Co-Chief Scientist
Scripps Institution of Oceanography
University of California, San Diego
9500 Gilman Drive
La Jolla CA 92093-0225
USA
dblackman@ucsd.edu
Work: (858) 534-8813
Fax: (858) 534-5332

Benoit Ildefonse
Co-Chief Scientist
Laboratoire de Tectonophysique
Université Montpellier II
CC49
34095 Montpellier
France
benoit@dstu.univ-montp2.fr
Work: (33) 46714-3818
Fax: (33) 46714-3603

Barbara E. John
Co-Chief Scientist
Department of Geology and Geophysics
University of Wyoming
1000 East University Avenue
Department 3006
Laramie WY 82071
USA
bjohn@uwyo.edu
Work: (307) 766-4232
Fax: (307) 766-6679

Yasuhiko Ohara
Co-Chief Scientist
Ocean Research Laboratory
Hydrographic and Oceanographic Department of Japan
5-3-1 Tsukiji, Chuo-ku
Tokyo 104-0045
Japan
ohara@jodc.go.jp
Work: (81) 3-3541-4387
Fax: (81) 3-3541-3870

D. Jay Miller
Expedition Project Manager/Staff Scientist
Integrated Ocean Drilling Program
Texas A&M University
1000 Discovery Drive
College Station TX 77845-9547
USA
miller@iodp.tamu.edu
Work: (979) 845-2197
Fax: (979) 845-0876

Christopher J. MacLeod
Shore-based Contributor
School of Earth, Ocean and Planetary Sciences
Cardiff University
Main Building, Park Place
Cardiff CF10 3YE
United Kingdom
MacLeod@cardiff.ac.uk
Work: (44) 29-208-74332
Fax: (44) 29-208-74326

Expedition 304 Scientific Party

Florence Einaudi
Logging Staff Scientist
Laboratoire de Géophysique et Hydrodynamique en Forage
Université Montpellier II, ISTEEM
Case Courrier 56
34095 Montpellier Cedex 5
France
einuaudi@dstu.univ-montp2.fr
Work: (33) 4-67-14-93-09
Fax: (33) 4-67-14-93-08

Michael W. Abratis
Metamorphic Petrologist
Institute for Geosciences
University of Jena
Burgweg 11
07749 Jena
Germany
michael.abratis@uni-jena.de
Work: (49) 3641-948-721
Fax: (49) 3641-948-602

Eric S. Andal
Igneous Petrologist
Department of Earth Sciences
Kanazawa University
Kakuma-machi
Kanazawa City, Ishikawa 920-1192
Japan
andal_es@earth.s.kanazawa-u.ac.jp
Work: (81) 076-264-5726
Fax: (81) 076-264-5746

Muriel Andreani
Metamorphic Petrologist
Laboratoire de Geosciences Marines
CNRS UMR 7097
Institut de Physique du Globe de Paris
4 Place Jussieu—Case 89
75252 Paris Cedex 5
France
Andreani@ipgp.jussieu.fr
Work: (33) 1-44-27-5193

Shunsaku Awaji
Geochemist
Department of Geosystem Engineering
The University of Tokyo
7-3-1 Hongo
Bunkyo-ku, Tokyo
Japan
Tt36508@mail.ecc.utokyo.ac.jp
Work: 81-3-5841-7019

Allison Charney
Igneous Petrologist
University of Connecticut
Geology and Geophysics Department
354 Mansfield Road, U-45
Storrs CT 06269-2045
USA
Allison.charney@uconn.edu
Work: (860) 486-0606
Fax: (860) 468-1383

David Christie
Igneous Petrologist
College of Oceanic and Atmospheric Sciences
104 Ocean Administration Building
Oregon State University
Corvalis OR 97331-5503
USA
dchristie@coas.oregonstate.edu
Work: (547) 737-5205
Fax: (547) 737-2064

Marion Drouin
Metamorphic Petrologist
Laboratoire de Tectonophysique
Université Montpellier II
Case Courrier 49
Place Eugène Bataillon
34095 Montpellier Cedex 5
France
marion.drouin@dstu.univ-montp2.fr
Work: (33) 4-67-19-39-41
Fax: (33) 4-72-44-8382

Bryce R. Frost
Metamorphic Petrologist
Department of Geology and Geophysics
University of Wyoming
1000 East University Avenue
Laramie WY 82071
USA
rfrost@uwyo.edu
Work: (307) 766-4290
Fax: (307) 766-6679

Jeffrey S. Gee
Paleomagnetist
Geosciences Research Division
Scripps Institution of Oceanography
University of California, San Diego
Mail code 0220
La Jolla CA 92093-0220
USA
jsgee@ucsd.edu
Work: (858) 534-4707
Fax: (858) 534-0784

Marguerite Godard
Geochemist
Laboratoire de Tectonophysique
Université Montpellier II
Case Courrier 49
Place Eugène Bataillon
34095 Montpellier Cedex 5
France
margot@dstu.univ-montp2.fr
Work: (33) 467-14-39-37
Fax: (33) 467-14-36-03

Craig B. Grimes
Structural Geologist
Department of Geology and Geophysics
University of Wyoming
1000 East University Avenue
Laramie WY 82071
USA
cgrimes@uwyo.edu

Nicholas W. Hayman
Structural Geologist
Division of Earth and Ocean Sciences
Duke University
103 Old Chemistry Building
Durham NC 27708-0230
USA
hayman@duke.edu
Work: (919) 681-8165
Fax: (919) 684-5833

Takehiro Hirose
Structural Geologist
Department of Geology and Mineralogy
Graduate School of Science
Kyoto University
Kyoto 606-8502
Japan
hirose@kueps.kyoto-u.ac.jp
Work: 81-75-753-4150
Fax: 81-75-753-4189

James Gregory Hirth
Structural Geologist
Department of Geology and Geophysics
Woods Hole Oceanographic Institution
MS 8
Woods Hole MA 02543
USA
ghirth@whoi.edu
Work: (508) 289-2776
Fax: (508) 457-2183

Jinichiro Maeda
Igneous Petrologist
Division of Earth and Planetary Sciences
Graduate School of Science
Hokkaido University
N10W8 Kita, Sapporo
Hokkaido 060-0810
Japan
jinmaeda@ep.sci.hokudai.ac.jp
Work: 81-11-706-4639

Andrew M. McCaig
Metamorphic Petrologist
Earth Sciences, School of Earth and Environment
University of Leeds
Leeds LS2 9JT
United Kingdom
andrew@earth.leeds.ac.uk
Work: (44) 113-3435219
Fax: (44) 113-3435259

Antony Morris
Paleomagnetist
School of Earth, Ocean, and Environmental Sciences
University of Plymouth
Drake Circus
Plymouth PL4 8AA
United Kingdom
amorris@plymouth.ac.uk
Work: (44) 1752-233120
Fax: (44) 1752-233117

Tatsunori Nakagawa
Microbiologist
Graduate School of Science
Department of Mineralogy, Petrology, and Economic Geology
Tohoku University
Aoba, Aramaki-Aza
Aoba-ku, Sendai
Miyagi 980-8578
Japan
n-takko@ganko.tohoku.ac.jp
Work: (81) 22-217-6660
Fax: (81) 22-217-6660

Roger C. Searle
Physical Properties Specialist
Department of Earth Sciences
University of Durham
South Road
Durham County
Durham DH1 3LE
United Kingdom
r.c.searle@durham.ac.uk
Work: (44) 191-334-2307
Fax: (44) 191-334-2301

Anette von der Handt
Igneous Petrologist
Abeilung Geochemie
Max-Planck-Institut für Chemie
PO Box 3060
55020 Mainz
Germany
avdhandt@mpch-mainz.mpg.de

Expedition 305 Scientific Party

Heike Delius
Logging Staff Scientist
Department of Geology
University of Leicester
University Road
Leicester LE1 7RH
United Kingdom
hd21@le.ac.uk
Phone: (44) 116-252-3634
Fax: (44) 116-252-3918

Natsue Abe
Igneous Petrologist
Deep Sea Research Department
Japan Marine Science and Technology Center
2-15 Natsushima-cho
Yokosuka, Kanagawa 237-0061
Japan
abenatsu@jamstec.go.jp
Work: (81) 46-867-9329
Fax: (81) 46-867-9315

James S. Beard
Metamorphic Petrologist
Department of Earth Sciences
Virginia Museum of Natural History
1001 Douglas Avenue
Martinsville VA 24112
USA
jbeard@vmnh.net
Work: (276) 666-8611
Fax: (276) 632-6487

Daniele Brunelli
Igneous Petrologist
Laboratoire Pierre Süe–DRECAM
CNRS
91191 Yvette Cedex
France
brunelli@drecam.cea.fr
Work: (33) 1-6908-9522
Fax: (33) 1-6908-6923

Adélie G. Delacour
Metamorphic Petrologist
Institut für Mineralogie und Petrographie
Eidgenössische Technische Hochschule - Zentrum
Sonnegstrasse 5
Zürich 8092
Switzerland
adelie.delacour@erdw.ethz.ch
Work: (41) 1 632 7823
Fax: (41) 1 632 1088

Javier Escartin
Structural Geologist
Marine Geosciences
Université Pierre et Marie Curie
Case 89 IPGP
4 Place Jussieu
75252 Paris
France
escartin@ipgp.jussieu.fr
Work: (33) 1-4427-4601
Fax: (33) 1-4427-9969

Patricia B. Fryer
Metamorphic Petrologist
School of Ocean and Earth Science and Technology
University of Hawaii at Manoa
1680 East-West Road
Honolulu HI 96822
USA
pfryer@hawaii.edu
Work: (808) 956-3146
Fax: (808) 956-6322

Angela Halfpenny
Structural Geologist
Department of Earth and Ocean Studies
University of Liverpool
4 Brownlow Street
Liverpool, Merseyside L69 3GP
United Kingdom
a.halfpenny@liverpool.ac.uk
Work: (44) 151-794-5174
Fax: (44) 151-794-5196

Heidi-Elisabeth Hansen
Igneous Petrologist
Department of Earth Science
University of Bergen, Norway
Allegaten 41
Bergen
Norway
st08759@student.uib.no
Work: (47) 5531 3949

Amber C. Harris
Physical Properties Specialist
Graduate School of Oceanography
University of Rhode Island
Narragansett RI 02882
USA
aharris@gso.uri.edu
Work: (401) 241-6874

Akihiro Tamura Hasebe
Igneous Petrologist
Department of Earth Sciences
Kanazawa University
Kakuma, Kanazawa 920-1192
Japan
kamui@kenroku.kanazawa-u.ac.jp
Work: (81) 76 264 5723
Fax: (81) 76 264 5746

Eric Hellebrand
Igneous Petrologist
Abteilung Geochemie
Max-Planck-Institüt für Chemie
Postfach 3060
55020 Mainz
Germany
ehelle@mpch-mainz.mpg.de
Work: (49) 6131-305220
Fax: (49) 6131-371051

Satoko Ishimaru
Igneous Petrologist
Division of Environmental Science and Engineering
Kanazawa University
Graduate School of Natural Science and Technology
Kakuma, Kanazawa 920-1192
Japan
jaja@earth.s.kanazawa-u.ac.jp
Work: (81) 76-264-5723
Fax: (81) 76-264-5746

Kevin T.M. Johnson
Igneous Petrologist
Department of Geology and Geophysics/SOEST
University of Hawaii at Manoa
1680 East-West Road
Post 606B
Honolulu HI 96822
USA
kjohnso2@hawaii.edu
Work: (808) 956-3444
Fax: (808) 956-5512

Garry D. Karner
Physical Properties Specialist
Lamont-Doherty Earth Observatory of Columbia University
PO Box 1000, 61 Route 9W
Palisades NY 10964
USA
garry@ldeo.columbia.edu
Work: (845) 365-8355
Fax: (845) 365-8156

Margaret Linek
Logging Trainee
Angeandte Geophysik
Rheinisch-Westfälischen Technischen Hochschule Aachen
RW Technische Hochschule
Lochnerstrasse 4-20
52064 Aachen
Germany
m.linek@geophysik.rwth-aachen.de
Work: (49) 241-809-4832
Fax: (49) 241-809-2132

Olivia U. Mason
Microbiologist
College of Oceanography
Oregon State University
Giovannoni Laboratory
104 COAS Administration Building
Corvallis OR 97331-5503
USA
omason@coas.oregonstate.edu
Work: (503) 939-1035

Katsuyoshi Michibayashi
Structural Geologist
Institute of Geosciences
Shizuoka University
Faculty of Science
836 Oya
Shizuoka 422-8529
Japan
sekmich@ipc.shizuoka.ac.jp
Work: (81) 54-238-4788
Fax: (81) 54-238-0491

Toshio Nozaka
Metamorphic Petrologist
Department of Earth Sciences
Okayama University
3-1-1 Tsushima-naka
Okayama 700-8530
Japan
nozaka@cc.okayama-u.ac.jp
Work: (81) 86-251-7883
Fax: (81) 86-251-7895

Martin Rosner
Geochemist
Department of Marine Chemistry and Geochemistry
Woods Hole Oceanographic Institution
Clark Building, MS 23
Woods Hole MA 02543
USA
mrosner@whoi.edu
Work: (508) 289-2699
Fax: (508) 457-2193

Guenter Suhr
Structural Geologist
Mineralogisch-Petrographisches Institut
Universität Köln
Zülpicher Strasse 49b
50674 Köln
Germany
suhr@min.uni-koeln.de
Work: (49) 221-470-3196
Fax: (40) 221-470-5199

Masako Tominaga
Paleomagnetist
Department of Oceanography
Texas A&M University
3F Oceanography Building
3146 TAMU
College Station TX 77843-3146
USA
masako@ocean.tamu.edu
Work: (979) 845-7211
Fax: (979) 845-6331

Toru Yamasaki
Geochemist
Inorganic Geochemist
Department of Earth and Planetary Sciences
Hokkaido University
Graduate School of Science
N 10, W 8
Sapporo, Hokkaido 060-0810
Japan
toru@ep.sci.hokudai.ac.jp
Work: (81) 11 716 2111, ext. 4655
Fax: (81) 11 746 0394

Xixi Zhao
Paleomagnetist
Institute of Tectonics
University of California, Santa Cruz
1156 High Street
Santa Cruz CA 95064
USA
xzhao@es.ucsc.edu
Work: (831) 459-4847
Fax: (831) 459-3074

Transocean Officials

Pete Mowat
Master of the Drilling Vessel
Overseas Drilling Ltd.
707 Texas Avenue South, Suite 213D
College Station TX 77840-1917
USA

Tim McCown
Drilling Superintendent
Overseas Drilling Ltd.
707 Texas Avenue South, Suite 213D
College Station TX 77840-1917
USA

Industry Participant

Richard Goebel
Engineering
SDS Digger Tools
47-51 Vulcan Road
Canningvale
Perth WAS 6155
Australia
rcmgoebel@bigpond.com.au
Work: (61) 89 455 4433
Fax: (61) 89-455-4399

IODP Shipboard Personnel and Technical Representatives

Michael Storms
Supervisor of Operational Support

Stephen Midgley
Operations Superintendent

Burnette Hamlin
Laboratory Officer

Timothy Bronk
Assistant Laboratory Officer

Paul Teniere
Assistant Laboratory Officer

Christopher Bennight
Marine Laboratory Specialist: Chemistry

Lisa Brandt
Marine Laboratory Specialist: Chemistry

William Crawford
Imaging Specialist

Jason Deardorff
Marine Laboratory Specialist: X-Ray

Randy Gjesvold
Marine Instrumentation Specialist

Kevin Grigar
Drilling Engineer

Margaret Hastedt
Marine Computer Specialist

Jennifer Henderson
Marine Laboratory Specialist: Core Laboratory

Karen Johnston
Marine Laboratory Specialist:
Underway Geophysics

Peter Kannberg
Marine Laboratory Specialist: Downhole Tools/
Thin Sections

Deepak Kannoju
Programmer Specialist

Michael Meiring
Marine Instrumentation Specialist

David Morley
Marine Computer Specialist

Heather Paul
Marine Laboratory Specialist: Physical Properties

Jennifer Presley
Yeoperson

Steven Kittredge
Schlumberger Engineer

ABSTRACT

Seafloor drilling during Integrated Ocean Drilling Program Expedition 304 was designed to investigate the processes that control formation of oceanic core complexes (OCCs), as well as the exposure of ultramafic rocks in very young oceanic lithosphere. Prior studies indicated that two main drill sites on a 0.5–2 m.y. old OCC on the western rift flank of the Mid-Atlantic Ridge (MAR), 30°N, could provide key constraints on the structure of the detachment fault zone, rock types exposed at shallow structural levels in the footwall, and their alteration history, as well as that of the volcanic succession in the hanging wall. Site U1309 is located in the footwall of the central dome of Atlantis Massif, where drilling was quite successful. The goal of establishing a reentry hole for subsequent deep penetration on Expedition 305 was accomplished, and coring during Expedition 304 went well beyond the initial plan to reach ~120 mbsf. In the 400 m penetrated at Hole U1309D during Expedition 304, a series of interfingered gabbroic intrusions were distinguished based on variation in olivine content, the presence of intercumulus phases, the extent of late magmatic dikes, and the presence of oxide gabbro. The boundaries of these lithologic zones commonly coincide with structurally defined boundaries.

Overall, the composition of the gabbroic rocks from Hole U1309D is among the most primitive known along the MAR. Several meter-scale intervals of serpentinized peridotite were recovered, comprising ~5% of the total recovery. A few of these ultramafic intervals may represent residual mantle harzburgite, but many have a low Mg number (88.9–89.6), indicating they are cumulates and/or have been impregnated by later melts. Diabase and basalt are present only in the upper 130 m of the footwall and are tholeiitic in composition.

Drilling in the hanging wall, Sites U1310 and U1311, was only marginally successful. The operational approaches used in our attempts to establish a reentry hole did not work. The main result from the limited recovery at these sites is the finding that relatively fresh basalt is present near the boundary of the central dome and adjacent volcanic block. The composition of these basalts is primitive tholeiite.

Shallow penetration holes through the sediment carapace on the footwall and into basement provided fossiliferous ooze, hyaloclasite, and fragments of fault rock and metabasalt/diabase. These samples provide initial confirmation that the corrugated dome coincides with an exposed detachment fault. If dating of the sedimentary de-

posits is possible, some constraints on the timing of its exposure at the seafloor may be obtained.

The lack of widespread deformation in the upper 400 m sampled at Site U1309 suggests that strain is concentrated in a small number of very localized zones. Several aspects of the drill core change across these faulted zones: the nature of the intrusive sequence and its alteration history, the intensity of deformation and abundance of veins, and average paleomagnetic inclination angle. A monotonic decrease in deformation intensity and/or systematic rotation of the footwall, such as predicted by the rolling hinge model, is not recorded in the recovered core.

BACKGROUND AND OBJECTIVES

Atlantis Massif formed within the past 1.5–2 m.y., and it currently bounds the median valley on the western flank of the at Mid-Atlantic Ridge (MAR) 30°N (Fig. **F1**). The corrugated, striated central portion of this domal massif displays morphologic and geophysical characteristics inferred to be representative of an oceanic core complex (OCC) exposed via long-lived detachment faulting (Cann et al., 1997; Blackman et al., 1998, 2004; Collins et al., 2001). The "core" of the complex is composed of crust and possibly upper mantle rocks, denuded by a detachment fault exposed over an 8–10 km wide, 15 km long area that forms the elongate, doubly plunging domal seafloor morphology. An adjacent basaltic block to the east is interpreted as the hanging wall to the detachment fault. A thin cover of lithified sediment, volcanic deposits, and rubble on the dome of the massif impedes seafloor mapping and sampling of the fault surface. The sediment-draped volcanic morphology and basalt sampled from scarps in the eastern block show its general character; the location of its contact with the dome can only be inferred from the break in slope. The detachment is inferred to dip beneath the seafloor at the base of the dome and to continue at a shallow angle (<15°) beneath the eastern block.

Evolution of the southern portion of the massif may differ from that of the central dome. The southern ridge (Fig. **F1**) has experienced greater uplift, shoaling to 700 m below sea level (mbsl). There, the corrugated surface extends eastward to the top of the median valley wall. Exposures along the south face of the massif represent a cross section through the core complex. The serpentinization-driven Lost City hydrothermal vent field is just below the summit of the southern ridge (Kelley et al., 2001, 2003; Früh-Green et al., 2003).

Seismic refraction results at Atlantis Massif (Fig. **F2A, F2B**) (Detrick and Collins, 1998) indicate that velocities of 8 km/s occur within several hundred meters of the seafloor at least locally in parts of the core of the massif. The gradient of seismic velocity in the central dome of Atlantis Massif has been determined to be similar to that determined near Ocean Drilling Program (ODP) Site 920, where 100–200 m of serpentinized peridotite was drilled. The determined gradient is quite distinct from that characterizing gabbro-hosted Atlantis Bank (Southwest Indian Ridge) and other sections of the MAR.

Interpretation of multichannel seismic (MCS) reflection data suggests a major difference in structure between the outside (conjugate) corner lithosphere versus that host-

ing Atlantis Massif (Canales et al., 2004). The Layer 2a/2b boundary is quite clear on the eastern flank of the ridge axis, but it is not evident on the western flank across the massif. A strong reflector is visible at 0.2–0.5 s below much of the domal surface (Fig. **F2C, F2D**) and coincides roughly with the depth below which mantle velocities (~8 km/s) are deduced. One interpretation suggests that the reflector marks an alteration front within the peridotite-dominated massif (Canales et al., 2004).

Modeling of sea surface and sparse seafloor gravity data (Blackman et al., 1998, 2004; Nooner et al., 2003) suggests that rocks at depth beneath the dome have a density 200–400 kg/m^3 greater than the surrounding rock. Two-dimensional model results support the interpretation that the footwall is overlain by tilted hanging wall blocks capped by rocks with density typical of the upper crust (2.5–2.7 kg/m^3). The interface between the model blocks in the east is a gently inclined (15°–25°) boundary that dips more steeply than the exposed corrugated surface (~11°) where it meets that hanging wall, perhaps coinciding with the base of the fractured, highly altered detachment fault zone.

In situ rock samples from scarps, side-scan imagery, and gravity data suggest that the majority of the hanging wall block is composed of erupted basalt. Seismic data show a discontinuous but persistent reflector 0.2–0.5 s beneath the seafloor, which Canales et al. (2004) show coincides with the projection of the corrugated slope beneath the western edge of the hanging wall block. They interpret this reflector to be the unexposed detachment fault. Assuming an average velocity of 4 km/s in fractured basalt, the reflector is predicted to occur at 200–300 m below seafloor (mbsf) at the hanging wall drill site.

Rock samples collected by the manned submersible *Alvin* from the central dome are mostly angular talus and rubble of serpentinized peridotite, metabasalt, and limestone (Cann et al., 2001; Blackman et al., 2004). A few samples from the central dome show cataclastic deformation or are highly serpentinized and metasomatically altered peridotite. The protolith of most of the serpentinite sampled on the south wall is harzburgite. These rocks are commonly cut by highly altered gabbroic veins composed dominantly of talc, tremolite, and chlorite (Früh-Green et al., 2001; Schroeder et al., 2001). Low-temperature overprinting, seafloor weathering, and carbonate vein formation mark the youngest phases of alteration.

Microstructural analysis of samples from the south wall indicates shear deformation and dilational fracturing at metamorphic conditions ranging from granulite to sub-

greenschist facies (Schroeder et al., 2001). Ductile fabrics in peridotite samples are overprinted by semibrittle and brittle deformation (Schroeder and John, 2004). Stable mineral assemblages of tremolite, chlorite, and chrysotile indicate that the latter processes occurred at temperatures <400°C. The distribution of samples suggests that strong semibrittle and brittle deformation is concentrated at shallow structural levels (<90 m beneath the domal surface) at the southern ridge (Schroeder and John, 2004). Outcrop mapping with the *Alvin* and photomosaics constructed from Argo digital still camera shots show that this uppermost fault extends across much of the top of the southern ridge (Karson, 2003).

Scientific Objectives

Atlantis Massif has several key features that make it an ideal target for OCC drilling: it is less than 2 m.y. old, so weathering and erosion have not degraded (macro) structural relationships; the hanging wall is in contact with the footwall of the detachment; and mantle seismic velocity has been reported to occur at several hundred meters below seafloor of the domal core, affording access to fresh in situ peridotite with conventional drilling. Many fundamental questions about mantle melting can only been addressed in a limited way with the highly altered samples of oceanic peridotite available to date. If the geophysical data indicate the presence of residual mantle and drilling can recover these rocks, new insights would be gained on geochemical balances during melting, the nature of melt segregation and migration, and the rheology of the asthenosphere within the subaxial upwelling zone. This was a very high priority for the combined Expeditions 304 and 305, and the operational strategy was designed to maximize the chances for successful recovery of deep footwall rocks.

Hypotheses to be tested by drilling completed during Expeditions 304 and 305 are:

- A major detachment fault system controlled the evolution of Atlantis Massif.
- Significant unroofing occurred during formation of this OCC.
- Plate flexure (rolling hinge model) is the dominant mechanism of footwall uplift.
- The nature of melting and/or magma supply contributes to episodes of long-lived lithospheric faulting.
- Expansion associated with serpentinization contributes significantly to core uplift.
- Positive gravity anomalies at Atlantis Massif indicate relatively fresh peridotite.
- The Moho at Atlantis Massif is a hydration front.

Expedition 304 results allow testing of the first 4 hypotheses and Expedition 305 results are expected to address these as well as the last 3 hypotheses.

If long-lived normal faulting and displacement are responsible for the evolution of the massif, uplift of the core may be the result of isostatic adjustment (Vening Meinesz, 1950) and thin-plate flexure (Spencer, 1985; Wernicke and Axen, 1988; Buck, 1988; Lavier et al., 1999). Differential rotation between the footwall and hanging wall blocks is predicted by thin-plate theory, so we apply the Integrated Ocean Drilling Program (IODP) results to investigate whether the core/logging data show evidence of such history. Logging data provide continuous (oriented) images of fracture patterns in the borehole wall. These are compared with fractures and veins measured in the cores from the same depth interval. Paleomagnetic data are incorporated to determine any history of rotation of the upper footwall. The pressure/temperature evolution of alteration reflect the tectonic and magmatic history as well, with cooling rates and water/rock ratios being controlled by intrusions, the amount of unroofing, and the degree of fracturing.

Any detachment model predicts that hanging wall rocks initially reside structurally above the footwall. If this is the case, petrologic and geochemical results are expected to show a genetic relationship between footwall rocks and basalts of the hanging wall.

The processes responsible for the development of OCCs appear to be episodic, with one factor being the level or style of magmatic activity at the local spreading center. Detailed study of the igneous sequence and structural relationships therein will be used to address the evolution of melting, intrusion, and cooling during the formation of Atlantis Massif. Comparison of our findings with those from ODP Hole 735B, Leg 153, and Leg 209 provide a means for assessing the similarities and differences in conditions that prevailed at the (slow) spreading centers where the lithosphere drilled at these sites was initially formed.

FOOTWALL SITE

Site U1309 is located on the central dome of Atlantis Massif, 15 km west of the median valley axis of the MAR, where the seafloor coincides with what is interpreted to be a gently sloping, corrugated detachment fault surface. Two drill holes at this site (Holes U1309B and U1309D) penetrate a multiply intruded and faulted crustal section, providing core that documents the interplay between magmatism and deformation prior to, during, and subsequent to a period of footwall displacement and

denudation associated with detachment faulting. Five shallow penetration holes (Holes U1309A and U1309E–U1309H) were designed to sample the sedimentary carapace and upper few meters of the basement, to test the hypothesis that the upper surface coincides with the detachment fault, and to help constrain the temporal history of denudation. Collected sedimentary deposits may provide constraints on the timing of exposure across the dome based on the age and isotopic character of preserved microfossils. Basement rock sampled in these short holes provides initial information on deformation and alteration within the exposed fault and, perhaps, rock adjacent to the fault zone.

Site selection was based on a combination of geological and geophysical data, balancing the details of seafloor character with larger-scale objectives attainable if deep penetration of the footwall is successful. Centered within the gently sloping, morphologically corrugated, striated dome (Cann et al., 1997), the site coincides with gravity anomaly and seismic velocity maxima that indicate unaltered ultramafic rocks are likely to be present within several hundred meters below the seafloor (Blackman et al., 1998; Collins et al., 2001). Argo II imagery and *Alvin* dive mapping previously showed that the seafloor is covered by a thin layer of unconsolidated sediment, deposited on bedrock and in places interrupted by lineated rubble fields (Blackman et al., 2004). In areas without significant loose sedimentary cover, a thin cover of lithified carbonate caps the underlying low-relief basement. Dredge and *Alvin* sampling indicate that loose, angular fragments on the central dome include low-grade metabasalt and serpentinite (Blackman et al., 1998, 2004).

Site U1309 comprises eight holes drilled within 2 km of one another and along a spreading-parallel corridor (Fig. **F3**). The first five holes, Holes U1309A–U1309E, are located within 30 m of each other, in an area with 2–4 m of unconsolidated sedimentary deposits above basement. A 60 m × 50 m survey with the vibration-isolated television (VIT) camera on the drill string documented a ~2000 m² area where both a single-bit pilot hole and a deep penetration hole could be initiated within an area free of cobble- to boulder-sized rubble. The area is ~280 m south of an Argo II track (run 039) and an *Alvin* dive (3642), both from cruise AT3-60 (Blackman et al., 2004), just south of NOBEL line 10 and west of EW0102 MCS Line Meg-4, at common midpoint 4100 (Canales et al., 2004). Towed ocean-bottom instrument (TOBI) and DSL120 sidescan sonar data show spreading-parallel striations crossing this area. A gentle northeast slope coincides with the southern flank of the corrugation the site penetrates. Principal geologic results from the pilot and deep penetration holes are presented in subsequent sections of this summary.

The series of shallow penetration holes included in this footwall site are located adjacent to, 280 m northwest of, and 1.6 km northeast of the deep hole (Hole U1309D). The motivation for this series of holes is two-fold: first, to check for possible fossils or isotopic signatures in the sedimentary deposits to constrain the exposure age of the hypothesized detachment fault and, second, to attempt recovery of possible fault rock at the top of the domal surface. The first shallow penetration core was obtained in Hole U1309A. Overcoring in the top interval of the deep penetration holes (U1309B and U1309D) precluded meaningful recovery from the sedimentary deposits and several meters of basement immediately below. Additional shallow penetration holes were drilled in an effort to achieve that goal (Holes U1309E–U1309H).

Hole U1309A

Before initiating coring in Hole U1309A (30°10.1081′N, 42°07.1101′W; 1642 mbsl), we obtained a temperature measurement and seawater sample for microbiology and geochemistry. Bottom water at this site has temperature = 5.33° ± 0.6°C, pH = 7.73, alkalinity = 2.16 mM, and salinity = 35.5 g/kg. These values are typical for the water depth and North Central Atlantic location of the site. A push core in Hole U1309A (Table **T1**) recovered ~2.5 m of unlithified tacky mud above bedrock. This microfossil ooze (with foraminifers and pteropods) includes mineral grains (fresh olivine and pyroxene), as well as fish remains. A sample of sediment for microbiological study was collected from Section 304-U1309A-1R-2, 48–60 cm, ~20 cm above basement.

Hole U1309B

In an effort to assess drilling conditions and begin geologic characterization of the expected detachment fault zone, a single-bit pilot hole was drilled at Site U1309. Hole U1309B, cored at the same location as Hole U1309A, was cored to 101.8 mbsf. Recovery was good (overall average = 46%), increasing significantly (to an average of 52% for 30–100 mbsf) below the upper, very slow-drilling 25 m. The hole deviates from vertical by 7° toward the northeast, and this was probably a factor in the reduced quality for one of the downhole logging measurements.

Hole U1309C

The attempt to set casing for the hard rock reentry system was not successful in Hole U1309C (30°10.1081′N, 42°7.1209′W; 1638 mbsl). The hole was abandoned with ~25

m of 13⅜ inch casing pipe standing above the seafloor; it is 20 m east of Hole U1309B and ~30 m southwest of Hole U1309D.

Hole U1309D

Drilling in Hole U1309D (30°10.1195′N, 42°07.1131′W; 1645 mbsl) took place over two periods for a total of 15 days during Expedition 304; penetration reached 401.3 mbsf. The hole was spudded using a hammer drill with 13⅜ inch casing, in an effort to provide stable reentry for a deep hole. No rock was recovered in the upper 20.5 m of the hole. Below 20.5 mbsf, coring was accomplished using a rotary core barrel (RCB) bit. Despite rough sea conditions that were experienced during some of the drilling, recovery rates were very good—58% overall. The section from 108 to 126 mbsf (Cores 304-U1309D-18R to 21R) had very low recovery, including one empty core barrel, and a second with only 14% recovery. Logging data suggest this low recovery zone may coincide with a fault zone. Aside from the low recovery interval and the upper 30 m, recovery rates averaged 68%. As drilling conditions in the pilot hole (Hole U1309B) were very good, casing below 20 m in Hole U1309D was deemed unnecessary. This gave us time to core the upper ~100 m during our initial occupation of the hole, providing an opportunity to assess cross-hole correlation of lithologic units and structure. The second period of coring followed drilling at Sites U1310 and U1311 and deepened the hole to 401.3 mbsf.

Hole U1309E

Hole U1309E (30°10.1207′N, 42°07.1057′W; 1645 mbsl) was offset 10 m east of Hole U1309D for an attempt to recover the sediment and upper meter of basement using the RCB. Disrupted sediments were obtained, as were several fragments of metabasalt.

Hole U1309F

The second attempt at shallow penetration was made in Hole U1309F (30°10.1999′N, 42°07.2518′W, 1645 mbsl) ~280 m to the northwest of Hole U1309D in an area where unconsolidated sedimentary deposits are less widespread than at the sites of Holes U1309A–U1309E, and lithified carbonate cap rock was mapped with the *Alvin* and Argo during cruise AT3-60 in 2000. A brief camera survey confirmed the basic setting, although some loose sediment occurred within a few meters of the first contact of the drill bit at the seafloor. Despite clear indications that we drilled over a meter into hard rock, recovery included only disrupted sediment and a few fragments of metabasalt.

No chips of lithified carbonate were recognized. We discontinued RCB shallow penetration attempts and switched to the extended core barrel (XCB) bit for the next attempt.

Hole U1309G

Hole U1309G (30°10.5379′N, 42°06.3179′W; 1872 mbsl) was sited 1.6 km northeast of Hole U1309D, in an area characterized by a broad region of variably lithified carbonate deposits above basement. A brief camera survey confirmed this assessment, and the hole was located within site of a marker left by the *Alvin* in 2000. The hole was spud into stepped and platy, lithified carbonate sediment. Coring to 3.5 m using an XCB bit recovered 0.91 m of microfossil ooze, with three thin (2–3 cm) interlayers of basaltic hyaloclastite. Glass from the hyaloclastite is oxidized palagonite. No lithified carbonate or intact basement rock was recovered. The sequence of fossiliferous ooze, hyaloclastite, and a clayey material with rounded, largely metabasalt clasts may provide useful post-exposure data. The latter could be a sedimentary conglomerate, but we cannot rule out significant reworking due to drilling in this lowermost interval.

Hole U1309H

A second attempt at basement recovery from a shallow penetration hole at the same location as Hole U1309G was possible when logging activities in Hole U1309D were stopped early due to tool hang-ups apparently associated with falling rock. Rather than risk either the tools or hole, the remaining time on site was used to RCB core a few meters at essentially the same location as Hole U1309G. This eliminated the need for camera survey. Drilling for 4 h penetrated to 4 mbsf; recovery from this hole was 0.19 m and includes pieces of basalt and talc-tremolite schist along with one piece of diabase cataclasite (Fig. **F4**). Despite the small return, these samples are significant. The talc-tremolite schist is similar to fault rocks recovered near the top of the southern ridge at Atlantis Massif (Schroeder and John, 2004) and at 15°45′N on the MAR (Escartin et al., 2003). Fracture intensity in the diabase is minor, suggesting fairly low strain, but consistent with the sample being part of a process zone associated with a fault system. Although these samples are minimal, they provide the first direct evidence that the corrugated central dome of Atlantis Massif is an exposed detachment. An *Alvin* sample within this spreading-parallel corridor showed similar talc rock (Blackman et al., 2004), and there were a few chips of talc-tremolite schist in the top core from Hole U1309B, but neither of these samples could be proven to be in place.

Prior confirmation of the existence of a fault zone capping the dome had been available on the southern ridge where microstructural analysis of dive samples (Schroeder and John, 2004) showed a 50–100 m thick zone where brittle deformation was concentrated just below the top of the south face of the massif.

A total of 12 samples for microbiological investigations were taken from core recovered from Holes U1309B and U1309D. Sample depths ranged from 0.45 to 396.5 mbsf, and all major rock types were included: carbonate sediment, basalt, diabase, gabbro, and serpentinized peridotite. Onboard cultivation studies indicate growth of matter from two altered gabbro samples at elevated temperature, based on positive fluorescence tests. Onshore analyses are required confirm that this is a microbial signature as opposed to being due to inorganic material.

Intrusive Sequence

Igneous rocks recovered from Holes U1309B and U1309D on the central dome of Atlantis Massif record a series of intrusions likely to have occurred at a variety of depths within the subaxial zone of the spreading center and, perhaps, into young lithosphere as it was incorporated in the western flank of the rift axis (Fig. **F5**). Mafic rocks recovered at Site U1309 fall into six major rock types: basalt and diabase, gabbroic rocks including oxide gabbro, gabbro, olivine and troctolitic gabbro, and troctolite. Ultramafic rocks recovered at Site U1309 are, in general terms, serpentinized peridotite, their composition ranging from residual mantle harzburgite and dunite to cumulate dunite, wehrlite, lherzolite, and olivine-rich troctolite. All ultramafic rocks have undergone hydrothermal alteration and are multiply intruded by later gabbro dikes and/or veins. In the upper 100 m interval cored in both Holes U1309B and U1309D, gabbroic rocks make up 50%–60% of the recovered section, basalt and diabase 40%–50%, and serpentinized peridotite ~0.5%–3% total (Fig. **F6**). Of the 401 m penetrated in Hole U1309D, 87% of the rock recovered is gabbroic, <10% is basalt and diabase, and 4% is serpentinized peridotite.

Basalt and diabase are restricted to the upper part of the footwall at Site U1309. No in situ diabase was recovered below ~127 mbsf during Expedition 304 (Fig. **F5**). Their intrusive contacts, taken with the relative intensity of alteration and vein development, suggest that the diabase bodies were emplaced late in the intrusive history of the footwall at Site U1309. Subhorizontal magmatic foliation, taken with paleomagnetic and logging data, suggest that diabase in Holes U1309D and U1309B forms groups of subhorizontal sheets or sills (Fig. **F7**). Unit boundaries are locally marked by chilled mar-

gins, and in some cases magnetic susceptibility varies systematically toward the top/base of a unit (Fig. F8). Together, these observations suggest individual sheet thicknesses on the order of 2–8 m. The basalt and diabase from Site U1309 are tholeiitic basalts to basaltic andesite, with compositions that overlap basaltic glasses from the entire MAR (Fig. F9). All samples analyzed are slightly CaO and Al_2O_3 poor, and Na_2O rich, compared to average MAR basaltic glass compositions. These differences may be related to the pervasive greenschist facies alteration.

Gabbroic rocks recovered at Site U1309 during Expedition 304, including troctolite, olivine gabbro, gabbro, and oxide gabbro, are grouped into 10 zones based on olivine content and the proportion of intercumulus phases present. Within each zone, one rock type is dominant, although others are commonly present as magmatic and/or intrusive layers ranging from a few centimeters to many tens of centimeters in thickness (Fig. F5). Grain sizes vary from fine to very coarse and locally pegmatitic. The thickness of each zone varies from ten to many tens of meters. This gabbroic section (>300 m thick) is cut by numerous thin late-magmatic leucocratic dikes, representing a late episode of intrusion of fractionated magma (Fig. F10).

The gabbroic rocks from Site U1309 have compositions that are among the most primitive sampled by drilling along the MAR (23°N and 15°20′N, Agar et al., 1997; Kelemen, Kikawa, Miller, et al., 2004) and on the Southwest Indian Ridge (ODP Hole 735B) (Dick, Natland, Miller, et al., 1999, Fig. F11). This is reflected in Mg numbers ranging from 74 to 90 and low TiO_2, Na_2O, and trace element contents. Most of the compositional variation observed in gabbroic rocks from Site U1309 is consistent with a simple mass balance involving increases in the proportion of clinopyroxene (or olivine in the troctolite) with decreases in the oxides that correspond to plagioclase (CaO, Al_2O3, Na_2O). Site U1309 gabbroic rocks are therefore interpreted as cumulates related to the basalt and diabase through crystal fractionation processes and a common parental magma.

Thermal demagnetization data show multiple components of remanence in several olivine gabbro and troctolite samples. The reversed magnetization component that characterizes most of the rocks from Site U1309 is overprinted by a normal polarity component with moderate inclination. The highest stability magnetization component in these samples is typically of reversed polarity and is isolated at temperatures above 520°–550°C. A lower stability normal polarity overprint is typically removed over the temperature range of ~350°–520°C. Such overprinting indicates reheating of the rocks, most likely associated with magmatic intrusion. Shipboard analyses show

that this occurred in several intervals cored in Hole U1309D; more detailed onshore analyses may provide paleomagnetic limits for the timing of such events.

Ultramafic rocks recovered at Site U1309 are of two types: those that may have been formed by cumulate igneous processes and, thus, may be part of the gabbroic section discussed above (Fig. **F12A**) and those that lack cumulate textures (Fig. **F12B**). The latter have bulk rock characteristics that suggest a residual mantle origin (high Mg and Fe content and low SiO_2, Al, and Na content), but these sections are too serpentinized for this conclusion to be certain based on shipboard observations; onshore analysis can provide key data.

Two short intervals of ultramafic rock were recovered in the upper 100 m of both Holes U1309B and U1309D. Four intervals of serpentinized peridotite (three of which are clearly in place) at ~61, 132.5, 172–173, and 224 mbsf were recovered in Hole U1309D and include both harzburgite and dunite. Harzburgites from Hole U1309B have Mg# (100 × molar Mg/[Mg+Fe]) of 90 and 91. The low CaO and Al_2O_3 contents of these harzburgites suggest that, prior to alteration, these peridotites were more refractory than those collected during Leg 153 at 23°N on the MAR (Casey et al., 1997). Ultramafic rocks from Hole U1309D include wehrlite from ~61 mbsf and dunite and harzburgite recovered from ~171 mbsf. The wehrlite is characterized by Mg# of 83, low Ti concentrations (<1 wt%), and high Fe_2O_3 (15 wt%). In contrast, ultramafic samples from deeper in the hole (Sections 304-U1309D-31R-1 and 31R-2 at 171 mbsf) have high Ca concentrations (1.15 wt%), Fe_2O_3 contents (10.03–10.84 wt%) and low Mg# (88.9–89.6). Barring possible calcium carbonate alteration, the two samples from intermediate depths in Hole U1309D are geochemically comparable to peridotite in Hole U1309B. As with Hole U1309B harzburgites, they are enriched in Fe compared to a global compilation of both abyssal peridotites and those tectonically emplaced with the same MgO concentrations.

Hydrothermal Alteration, Metamorphism, and Metasomatism

Alteration mineral assemblages in rocks from Site U1309 record cooling of mafic plutonic rocks from magmatic conditions (>1000°C) to the temperatures of zeolite facies (<200°C) during unroofing and denudation of Atlantis Massif. Many samples from the site, particularly those collected from below 350 mbsf in Hole U1309D, display little to no alteration (Fig. **F13**). Individual samples generally display a range of superposed metamorphic conditions, but no single sample records the entire cooling his-

tory of the site. The mineral assemblages encountered in any sample depend on at what point in its cooling history the rock underwent deformation and/or hydration.

The most extensive alteration event recorded at Site U1309 is hydration that took place at and below greenschist facies. Three distinct processes that occurred at temperatures below 500°C dominated this hydration. Static hydration at 400°–450°C formed characteristic tremolite-chlorite-talc corona textures (Fig. **F14**) along olivine/plagioclase interfaces and resulted in the formation of tremolite/actinolite from pyroxene in both gabbro and diabase. Plagioclase was stable except in the presence of olivine. The intensity of this hydration decreases with depth and is localized in and around small gabbroic dikes below ~350 mbsf. In another stage, localized fluid flow led to intense alteration associated with breccia zones above 60 mbsf and with late magmatic leucocratic dikes below ~160 mbsf. This alteration characteristically produced secondary plagioclase in addition to actinolite and, below 370 mbsf, epidote. This alteration episode occurred under conditions similar to the static alteration but generally appears to postdate it. In ultramafic rocks, this alteration produced talc-tremolite veins. Finally, in rocks where the coronitic reaction did not go to completion, fracture-controlled serpentinization of olivine is accompanied by replacement of plagioclase by prehnite and hydrogrossular at <350°C. This assemblage is rare above 300 mbsf, and apparently did not occur in rocks that are now above 130 mbsf, because either olivine or plagioclase was completely removed by the corona-forming reaction.

In addition to these dominant processes, pyroxene and plagioclase locally recrystallized in response to granulite-grade deformation. Hydration in the amphibolite facies is associated with ductile deformation in gabbro and in the margins of late magmatic leucocratic dikes. Hydration at clay grade (<100°C) appears along faults and fractures throughout the core but is not a pervasive phenomenon, and clays are only rarely seen in X-ray diffraction spectra of unfractured rock.

Talc-tremolite assemblages are common at contacts between ultramafic and mafic rocks (Fig. **F15**) and at dike contacts within the serpentinite. These contacts show greenschist facies metasomatism of peridotite by fluids rich in Si and Ca that have passed through and equilibrated with mafic rocks. The reciprocal metasomatic reaction in mafic rocks leads to complete chloritization of plagioclase and replacement of actinolite by tremolite. The same metasomatic reactions most likely produced the talc-tremolite-chlorite schists found in the uppermost cores of Holes U1309B, U1309D, and U1309F and by previous workers on the south side of Atlantis Massif

(Schroeder and John, 2004). In addition, hydrothermal fluids may be preferentially channeled along gabbroic intrusions as previously observed on the Mid-Atlantic Ridge (Cannat et al., 1992). Carbonate veins and replacement zones also appear in serpentinite close to contacts with gabbroic rocks and may reflect flow of fluid involved in serpentinization. The focused, serpentinization-driven fluid venting at the Lost City hydrothermal field, 5 km to the south of Site U1309, clearly indicates that this process takes place at Atlantis Massif. Variations in the strength of such flow would be expected as this oceanic core complex evolved.

Structural Relationships

Within the context of deformation expected for the footwall of a detachment at an oceanic core complex, the structural observations for Site U1309 show a somewhat surprising lack of deformation immediately below the hypothesized detachment fault exposed at the seafloor. Some localized high temperature deformation fabrics are observed. However, the amount of rock that is strongly deformed at high temperatures is relatively modest. The majority of the recovered cores show only evidence for greenschist grade semibrittle/brittle deformation associated with basaltic intrusions and hydrothermal alteration. In many cases, this deformation amounts to no more than a pervasive static alteration of the rock; pseudomorphs of igneous texture remain largely unmodified. These observations indicate that the exhumation of the uppermost Central Dome of Atlantis Massif was dominated by brittle and semibrittle processes associated with magmatic intrusions and extension.

Five structural units are identified in the uppder 400 m of Hole U1309D. The boundaries between these units coincide with boundaries between gabbroic zones defined by igneous relationships. The characteristic structural features that differ between the units, or approaching the boundary between units, are the intensity of cataclastic fabrics, the abundance of vein alteration, the intensity of crystal plastic fabric, and the amount of magmatic foliation (Fig. **F16**). Several aspects of the downhole logging data correlate wtih the stucturally defined unit. Caliper data indicate less clean hole conditions within many of the boundary zones (Fig. **F16H**), which are located in Hole U1309D at 135, 160, 260, and 285 mbsf. The boundary zone at ~160 mbsf is associated with relatively good hole conditions, but neutron porosity is high (Fig. **F16I**) and density is low (Fig. **F16J**) within this 5–10 m section of the borehole. The fact that several of the stuctural unit boundaries coincide with the thin screens of ultramafic rock leads us to suggest that they acted as zones of weakness during alteration and may have controlled the late denudation history of Atlantis Massif.

The early history of deformation recorded at Site U1309 is constrained by magmatic and crystal plastic deformation fabrics in ultramafic and gabbroic rocks. Crystal plastic deformation is localized into narrow shear zones (up to 30 cm thick) in both Holes U1309B and U1309D, with no significant change in style or distribution with depth. The highest density of shear zones is at 35–80 mbsf in Hole U1309D. Intervals deeper in the hole have discrete shear zones only a few centimeters thick. Crystal plastic deformation is clearly partitioned into more-fractionated gabbroic rock types but is generally lacking (only ~5% of the core showed such high-temperature deformation) in the 400 m section of the footwall transected in Hole U1309D during Expedition 304. This is in marked contrast to the significant deformation recorded in the upper 500 m of core recovered from ODP Hole 735B on the Southwest Indian Ridge (Dick, Natland, Miller, et al., 1999). The dip of the majority of crystal plastic shear zones at Site U1309 ranges from 20°–60° toward the west; at various depths subhorizontal dips occur as well.

Microstructures indicative of deformation by semibrittle processes at amphibolite-grade conditions in some parts of the section suggest small strains; the majority of the recovered core shows evidence of only greenschist-grade semibrittle/brittle deformation associated with basaltic intrusion and hydrothermal alteration. In many instances, this deformation amounts to no more than a pervasive static alteration; pseudomorphs of igneous texture remain largely unmodified. Alteration veins, fractures, cataclasite, and breccia record low-temperature brittle deformation. Tentative reorientation of structures using paleomagnetic and logging data indicate that the majority of veins dip toward the east and several faults strike east-west. These observations indicate that denudation of the upper central dome of Atlantis Massif was dominated by brittle and semibrittle processes associated with magmatic intrusion and extension. No structures indicative of high displacement by either ductile or brittle processes have been recovered to date. This result is significant, and it severely limits the possible thickness of fault zones that could comprise a detachment system on the central zone. Poor recovery of the the uppermost 20 m of the footwall leaves open the possibility that this narrow zone accommodated a very high strain along a brittle fault. Such extreme localization of strain has been documented to occur in continental detachments (John, 1987; Miller, 1996). If this is the case here, the central dome differs from the southern ridge of Atlantis Massif, where seafloor mapping and sample analysis suggest a detachment zone thickness on the order of 50–100 m (Schroeder and John, 2004).

The relatively undeformed nature of the plutonic section of the massif provides an unprecedented opportunity to study emplacement processes associated with formation of oceanic lithosphere over a wide range of magmatic conditions. The orientation of intrusive contacts, where preserved, are commonly subhorizontal to gently dipping—gabbro against peridotite and diabase against gabbro—suggesting a sheet or sill-like geometry of emplacement. In contrast, thin basaltic dikes typically have subvertical (65°–80°) contacts with chilled margins. Layering in the gabbro sequences from the upper parts of both Holes U1309B and U1309D is defined by variations in modal composition, grain size, or both (Fig. **F17**). Modal proportions of olivine and plagioclase vary over vertical intervals of centimeters. The observation of this layering in more primitive possibly cumulate-textured rocks indicates that melt migration was initially dominated by porous flow and compaction. In contrast, the observations of gabbro dikes and late magamatic leucocratic veins that cut more primitive rock types indicate that melt migration was controlled by brittle mechanisms during the late-stage fractionation and crystallization process. At the grain scale, the role of melt in promoting brittle processes is indicated by pyroxene crystals in oxide gabbros that are cut by veins filled with magmatic oxide and hornblende (Fig. **F18**). Finally, the observation of crystal-plastic shear zones within narrow intrusions/dikes and at the contacts between gabbroic intervals suggests that the presence of melt promoted strain localization during extension.

Paleomagnetic measurements on samples from Holes U1309B and U1309B show dominantly negative inclinations that represent reversed polarity remanence (Fig. **F19**). However, there are important downhole fluctuations in inclination. Average inclinations determined for core from <180 mbsf are approximately –45°, similar to the reversed polarity dipole inclination expected for this site. A pronounced reduction in inclination angle is evident in the interval from ~180 to 260 mbsf, where values are typically shallower than –30°; some rocks in this interval have shallow positive magnetic inclinations. At depths >260 mbsf, the inclinations again are steeper, though the average inclination is ~5°–10° shallower than those in the upper 180 m of the hole.

The reversed polarity magnetization components found at Site U1309, particularly from gabbro, provide a robust estimate of the geomagnetic field at the time the magnetization was attained. The mean inclination of the most reliable samples is –49.4° (+3.4°/–2.1°). Crosscutting relations between steeply dipping basaltic dikes and gently to moderately dipping faults, taken with the paleomagnetic data showing little difference in magnetic inclination (mean from most reliable gabbro samples = –51°) from the expected (–49°), suggests little horizontal axis rotation of the upper ~180 m at Site

U1309, the presumed upper part of the footwall to the fault system exposed at this location in the central dome.

The multicomponent remanence signatures discussed in the previous section potentially contain information on the thermal and tectonic history at Site U1309. The highest stability reversed polarity magnetization is shallower on average than the normal polarity overprint, although data scatter is also greater; the two components are not antipodal. The possible difference between the normal and reversed polarity directions may reflect the influence of tectonic tilting of the 180–260 mbsf interval after acquisition of the highest stability reversed polarity magnetization. In contrast, the mean inclination from the uppermost 180 m of Site U1309 (–48°) is essentially identical to that expected from a geocentric axial dipole (±49°), suggesting that this sequence experienced little tectonic rotation about horizontal axes. These shipboard results raise intriguing questions about the validity of the rolling hinge model for core complex formation. More complete onshore studies are necessary before final conclusions can be drawn.

HANGING WALL SITES

Taken together, the structural and preliminary paleomagnetic observations in the upper 400 m of the footwall of Atlantis massif suggest that models for core complex exhumation that require large viscous strains and footwall rotations need to be reevaluated. Structures indicative of high displacements by either ductile or brittle processes were not observed, and paleomagnetic data document a lack of significant tectonic rotation in the upper 120 m of the massif. Site U1310 was drilled to assess any petrogenetic relationship between volcanic rocks in the hanging wall and potential source rocks recovered in the footwall, to document faulting and any rotation of the hanging wall, and to compare the alteration and deformation styles between the footwall and hanging wall cores. The site was located where the hypothesized detachment that forms the corrugated central dome might be intersected once drilling reached the base of the hanging wall. The position of a seismic reflector (Canales et al., 2004) beneath Site U1310 may indicate that the detachment occurs at a depth of 250–350 mbsf. Recovery of rock from within the detachment zone was a high priority, inferred to be more likely where hanging wall volcanic rocks may armor the fault than at Site U1309, where seafloor exposure of the detachment is likely to have degraded (or even removed) the material due to weathering and/or erosion. In addition,

the difficulty associated with the bare-rock spud makes recovery of a thin detachment zone unlikely at the footwall site.

Because of drilling difficulties at Site U1310, we developed an alternate strategy for delivering some of the objectives outlined for the hanging wall site. Site U1311 is on the lower eastern slope of the central dome, along seismic Line Meg-10 (Canales et al, 2004), where the D-reflector is interpreted to surface before diving east beneath the hanging wall. The site can be interpreted as a possible klippe of hanging wall rock, stranded above the detachment fault. We note that if this target is not a klippe, but instead is either the detachment surface itself or post-exposure volcanic deposits, objectives related to penetration into D-reflector and into the footwall would still be addressed at this site.

Site U1310

Site U1310 is located ~9.3 km west of the center of the rift valley. TOBI and DSL120 side-scan sonar data and bathymetry indicate that the site is on a small fault-bound horst, ~600 m east of the break in slope inferred to mark the termination of the detachment fault exposed on the central dome. The site coincides with the eastern end of *Alvin* Dive 3643, Cruise AT3-60, in an area with numerous small northeast-striking scarps (both southeast and northwest facing) (Fig. **F20**). Based on nearby *Alvin* observations and sampling, these scarps expose pillow basalt.

A push test at the end of the camera survey indicated there was as much as 6 m of unlithified microfossil ooze in Hole U1301A (30°11.4850′N, 42°03.9256′W, 2583 mbsl). No coring was attempted at this site, but ~1 kg of broken basaltic material was recovered from the hammer drill casing when it returned to the rig floor. The dominant rock type is sparsely plagioclase-phyric fine-grained pillow basalt. A single ~10 cm pillow fragment has a palagonitized glass rim grading through a spherulitic zone to a microcrystalline interior. The remaining material ranges in size from ~5 cm to dust. It includes palagonitized glass fragments, some of which are encrusted by calcareous sediment and/or iron-manganese oxides, angular and drill-rounded fine-grained basalt fragments, and minor calcareous sediment and iron manganese oxides. The finer material includes separate fragments and coatings of ferrous and siliceous welding slag derived from assembly and disassembly of the bottom-hole assembly (BHA).

The first core recovered from Hole U1310B (30°11.4842′N, 42°03.9197′W; 2583.5 mbsl) contained 1.3 m of fist-sized and smaller pieces of basalt from the 13.5 m interval below a 5 m thick sediment cover. Although we cored as deep as 23 m, the second core barrel was still in the lower BHA when it severed, so no rock was recovered from below 18.5 mbsf. Most of the basalt fragments recovered from Core 304-U1310B-1R were broken, alteration along these fracture surfaces being minimal and the interior >1% altered, suggesting they are derived from in situ pillows. The piece interiors are also almost unaltered. Vesicles compose 3%–5% of the pieces analyzed. Vesicles close to fracture surfaces are internally discolored brown but not filled; spherulitic zones appear light brown in places, and within these zones, plagioclase appears white, rather than transparent. Some fragments have a glassy rim 1–3 mm thick, with relatively fresh glass. Thin zones of palagonite are mostly confined to the outer pillow surface. Glass samples were taken for onshore analysis prior to the postcruise sampling party.

In thin section, the pillow interiors appear fresh, with 5%–10% seriate plagioclase needles and radiating clusters in a glassy groundmass characterized by branching, feathery quench textures. Sparse anhedral olivine and prismatic plagioclase microphenocrysts are no more than 0.5 mm in size, with rare grains up to several millimeters in long dimension. Crystal clots composed of subophitic intergrowths of plagioclase and olivine are relatively common. Major and trace element geochemistry suggests that the basalt is a primitive tholeiite in composition. The basalt has 49.35 wt% SiO_2, 10.23 wt% MgO, 9.66 wt% Fe_2O_3, 15.21 wt% Al_2O_3, 11.94 wt% CaO, 2.02 wt% Na_2O, 0.05 wt% K_2O, and 0.95 wt% TiO_2. Site U1310 basalt has 7.8 ppm Ba, 72 ppm Sr, 23.9 ppm Y, 48.2 ppm Zr, 234 ppm V, and 34.3 ppm Sc. Sample 304-U1310B-1R-1, 16–18 cm, is characterized by high Mg and low trace element contents, consistent with the observation of olivine microphenocrysts noted in thin section.

Site U1311

Site U1311 is located on a small knoll near the break in slope where the corrugated dome meets the adjacent volcanic, hanging wall block. Recovery of fresh, glassy vesicular basalt in Hole U1311A does not provide a definitive test of the hypothesis that the site is located on a small klippe above the detachment fault, as outlined above. The eruptive basalt could have come from the inferred hanging wall, as hypothesized, or it could have been erupted onto or against the slope of the easternmost domal surface at anytime after exposure at the seafloor.

Hole U1311A (30°10.6091′N, 42°04.1904′W; 2552 mbsl) is located on the southern slope of the knoll. A 60 m × 60 m survey with the VIT camera documented a ~3600 m^2 area of mud- and rubble-covered seafloor, with a moderate slope to the south-southeast. Along the northeastern corner of the survey area, a moderately to steeply southeast-dipping, >20 m high scarp oriented east-northeast (~75°) crops out and is characterized by rounded pillow structures.

One attempt to drill at this site penetrated 12 mbsf, including 3.5 m of unconsolidated mud. Recovery from the hole produced 1.5 m (13%) of fresh, vesicular, moderately plagioclase-olivine phyric basalt pillows, with sparse glass preserved. Almost all pieces are angular and have broken along fracture surfaces within pillows—few, if any, were cut by the drill. The fracture surfaces are discolored dark brown and minimally altered. These observations suggest that the core is derived from in situ pillows. Some piece interiors include multiple gray Liesegang bands, indicating pervasive minor or incipient alteration. Vesicles close to fracture surfaces are internally discolored brown but not filled.

The basalt is dark gray to black in color and characterized by abundant (5%–10%) seriate plagioclase that locally occurs in radiating clumps. Sparse euhedral plagioclase phenocrysts range upward in size to ~2 mm. In thin sections from pillow interiors, the basalt appears fresh, with minimal darkening of the matrix and local occurrences of orange to green smectites either in vesicles or in the vicinity of olivine (Fig. **F21**). Randomly oriented, acicular to prismatic plagioclase, ranging in size from <0.1 to 0.5 mm, makes up ~40% of the sample. Many of the plagioclase crystals have hollow or swallowtail quench morphologies. Olivine microphenocrysts (~5%) appear either in subophitic crystal clots with plagioclase or as euhedral microphenocrysts ranging in size from 0.1 to 0.3 mm and in shape from larger prisms to smaller diamonds and more complex quenched forms. The remainder of the rock is the devitrified glass matrix, dominated by plumose, quenched clinopyroxene with anhedral interstitial plagioclase. Oxides are abundant, up to 2%, in the matrix and mostly occur as complex quench morphologies, most likely ilmenite. Vesicles occupy 3%–5% of total volume. They occur in two forms: round (~0.1 mm) and elongate, irregular, and locally interconnected. Most are unfilled, but a few are completely or partially filled by devitrified glass and a few, especially near fracture surfaces, are filled by secondary green or orange smectite. They generally range in size up to 0.5 mm, but in places are as large as 2 mm. Where present, glass is 1–3 mm thick with 50%–100% palagonitization close to outer surfaces.

The one sample of pillow basalt (Sample 304-U1311A-1R-1, 34–36 cm) analyzed for major and trace element geochemistry suggests that the basalt is a primitive tholeiite, with a Mg# of 66. The sample is characterized by loss on ignition values of –0.05 wt% and H_2O and CO_2 below detection limit. It has 48.97 wt% SiO_2, 9.63 wt% MgO, 9.82 wt% Fe_2O_3, 16.81 wt% Al_2O_3, 12.61 wt% CaO, 2.17 wt% Na_2O, 0.04 wt% K_2O, and 1.12 wt% TiO_2. The Site U1311 basalt has 8.8 ppm Ba, 83 ppm Sr, 26 ppm Y, 57 ppm Zr, and 38 ppm Sc, virtually equivalent to the basalt sampled in Hole U1310B. Basalt from both hanging wall sites reflect a depleted source.

PRELIMINARY SCIENTIFIC ASSESSMENT

The overall success of Expedition 304 is due to a combination factors.

- We far surpassed our goal for the first phase of drilling at the footwall site (proposed Site AMFW-01A; Site U1309). Average recovery rates were well above the average for all prior hard rock expeditions, although they were in line with rates from ODP Hole 735B, the only place deep penetration in a reentry hole can be compared.
- The sequence of intrusive rocks cored at this site and the high recovery rates provide an unexpected wealth of information on petrologic, alteration, and structural processes that characterize the magmatic construction of young oceanic crust at slow-spreading ridges.

A disappointing aspect of Expedition 304 is that we did not succeed in drilling more than ~20 mbsf in the hanging wall. The operational strategies employed, which were restricted because of loss of gear while setting the reentry system at the footwall site, were not adequate. Conceptually, it seems that the ring-bit spline drive hammer-in casing assembly would have provided a better start if it had been available. However, there is no guarantee that unstable conditions that might be dealt with by casing the upper 20–30 mbsf would not be just as problematic at any depth below the base of casing, because the hole would still be in fractured basalt. The minimal amount of rock recovered during a series of failed attempts to start a reentry hole in the hanging wall provides an intriguing glimpse of a compositional aspect of those rocks (see **"Site U1310"** and **"Site U1311"**), but not a conclusive test of the nature of the eastern volcanic block. Without significant recovery from the hanging wall, we cannot address petrogenetic relationships with the footwall rocks or the magnitude of hanging wall rotation relative to the footwall. In retrospect, this aspect of hanging wall studies might have been better served by simply attempting a series of single-bit holes, some of which might have been successful at achieving a few tens of meters penetration

and partial recovery. The goal of penetrating an unexposed portion of the detachment fault beneath the hanging wall was always a high-risk endeavor for Expedition 304. Once we recognized how difficult setting casing for the reentry system was in this environment, we adjusted the site location (from Site U1310 to Site U1311), in hopes that a small klippe covering the detachment could provide access to this second hanging wall objective with much less penetration. We (the engineers, drillers, staff scientist, and co-chiefs) worked hard to come up with an approach that would provide a workable reentry site in unsedimented, young basalt that characterized the sites; after 11 days it was clear that we could advance the objectives of the overall project more by returning to the footwall site.

Return to the footwall site allowed penetration to continue to over three times the original planned depth for Expedition 304. This bodes well for Expedition 305 objectives. Shipboard results are preliminary, but it is already clear that the structural and paleomagnetic data from Holes U1309B and U1309D will provide key constraints on the evolution of the footwall during formation of the OCC. At this (early!) stage, it is not clear how the classic "rolling hinge" model can explain the observations we have made on the core. Petrologic and geochemical data are equally intriguing, although for different reasons.

The relatively high proportion of gabbroic rocks recovered at Site U1309 on the central dome contrasts with recovery by dredge and submersible dives on the south wall of Atlantis Massif, which are dominated by serpentinized peridotite with gabbro making up only ~30% of those samples (Blackman et al., 1998, 2004). This discrepancy may simply reflect the difficulty of seafloor sampling from massive, undeformed exposures of possible gabbro, where subvertical outcrops up to 200 m high are cut by few fractures. Attempts to sample these sections with the *Alvin* were unsuccessful, so samples collected in 2000 were biased toward more fractured rocks, including those with well-developed foliation and/or fault rocks. Alternatively, it is possible that there are differences in the overall structure/composition between the southern ridge and the central dome, in which case the drill core provides important comparative data. Despite the high percentage of gabbroic rocks in Holes U1309B and U1309D being somewhat surprising, the recovered section provides an exceedingly rich data set for investigations on the petrogenesis and accretion history of ultramafic and mafic rocks generated at slow-spreading ridges. Because the petrology and alteration of the sequence varies on the scale of meters to a few tens of meters, relationships are available for study here that could not be addressed with prior ODP hard rock data.

EXPEDITION 304 OPERATIONS SUMMARY

Port Call

The Ponta Delgada, Azores Islands (Portugal), port call was completed in 3.5 days. Pacing items for the port call were loading of specialty hardware required for the advanced diamond core barrel system and the hard rock reentry system (HRRS), delayed incoming airfreight, and maintenance on the active heave compensator (AHC).

Transit to Site U1309 (Proposed Site AMFW-01A)

The last line away from Berth 12, Ponta Delgada, was at 2012 h on Saturday 20 November 2004. The transit was uneventful, with the ship averaging 11.1 kt over the 939 nmi distance. The vessel arrived at location (based on Global Positioning System coordinates) and launched a beacon at 0830 h on 24 November.

Site U1309 (Proposed Site AMFW-01A)

After arriving at Site U1309, we assembled the BHA and ran the pipe to just above the seafloor. Operations began with a VIT camera bottom survey to determine suitable locations to spud the pilot hole and to install the HRRS. The survey was completed in <2 h, and an appropriate area was selected for drilling (devoid of large boulders or rubble). A water sample and temperature measurement were collected with the Water Sampling Temperature Probe (WSTP) from just above the mudline. The first hole (Hole U1309A) was a punch core with the RCB assembly to capture the surface sediments. Rotary coring commenced in Hole U1309B (without moving ship location) at 0050 h on 25 November. Weight on bit started at 4000 lb with a rotation of 30 rpm and was gradually increased to 12,000 lb at 55 rpm as the BHA drilled into the hard formation. Penetration rates started at <1 m/h but increased to >2 m/h with the increased weight on bit and increased rotation. A brief test of the AHC system was conducted at the start of coring operations, but the vessel heave (4–5 m) proved too large for the AHC. Previous experience limits the use of the AHC to ~2.5 m maximum heave.

Coring continued to 101.8 mbsf (Table **T1**), when penetration ceased, likely owing to bit failure after >86 rotating hours. The mechanical bit release (MBR) was activated, and the bit was released at the bottom of the hole. The annulus was displaced with drill (fresh) water for logging and the pipe pulled back to 25 mbsf. Three logging runs were completed including the triple combo and FMS-sonic tool strings and a test of

the logging heave compensation winch. Logging was completed and operations in Hole U1309B ended at 0805 h on 1 December.

The HRRS was run in an attempt to install 31.5 m of casing in Hole U1309C, 20 m west of Hole U1309B. The hammer-in casing attempt started at 0945 h on 2 December. After ~5–6 m penetration, high torque and loss of pipe rotation dictated an inspection with the subsea camera. This inspection revealed that the casing running tool had prematurely released, disconnecting the BHA with the hammer from the casing string. With no further advancement possible, Hole U1309C was abandoned. A 25 m length of $13^{3}/_{8}$ inch casing was left sticking out of the seabed at Hole U1309C. A new drilling target (Hole U1309D) was selected, the HRRS system was prepared, and the vessel was offset 20 m north of Hole U1309B. Hole U1309D was spudded at 0120 h on 4 December. The HRRS was drilled to 20.5 mbsf, leaving 4.5 m of casing above the seafloor. After running the reentry cone, the VIT was deployed to inspect the HRRS. All components appeared to be in place. The BHA was pulled clear and tripped back to surface. An RCB BHA was then assembled to reenter Hole U1309D to core ahead from 20.5 mbsf.

The first reentry into Hole U1309D was accomplished in 10 min by 0240 h on 6 December. Cores 304-U1309D-1R to 22R (20.5–131.0 mbsf; recovery = 51%) were predominantly 4.5 m penetrations, but two ~9.5 m cores (Cores 16R and 17R; 89.0–107.9 mbsf) were cut to compare recovery rates. Penetration rates and operating parameters were similar to pilot Hole U1309B. Coring was terminated at 60.75 bit rotating hours to prevent bit deterioration from affecting hole conditions. After the bit cleared the top of the reentry cone at Hole U1309D, the vessel was moved to Site U1310 using the dynamic positioning (DP) system.

Site U1310 (Proposed Site AMHW-01A)

During the DP transit to Site U1310, drill pipe was added to reach the estimated 2580 m of water depth. A subsea camera survey located a target for Hole U1310A, and after a punch test to determine sediment thickness, the pipe was recovered. The bit cleared the rotary table at 1520 h on 10 December, officially ending Hole U1309D and starting Hole U1310A. The bit was in poor condition, with numerous missing and broken teeth and three loose cones.

The HRRS was assembled and tested at the rig floor prior to deployment. During the initial assembly, an error was discovered in the length measurement of the new

nonagon design bit. This resulted in the overall casing length being too short for the BHA. The bottom joint of casing had to be removed and the ring bit removed from the casing and reinstalled on a longer joint of casing. The completed assembly was then deployed to the seabed and a drill pipe measurement to the seafloor was recorded at 2594 meters below rig floor (mbrf). The HRRS was spudded at 0000 h on 12 December. Hammer drilling continued for the next 6.75 h with little penetration. The HRRS was pulled back to the surface, and it was clear that the nonagon design bit had failed. The drive bit had pushed through the ring bit and could not have been engaging during hammer operation. The nonagon pilot bit and nonagon ring bit were changed to a wing bit with an open casing shoe.

After 6 h during this HRRS installation attempt, penetration stopped and we were unable to maintain rotation. We pulled the hammer assembly from the seafloor, moved 10 m north, and attempted a third penetration. After 5 h, penetration stopped again with ~6 m of hole, so we pulled and inspected the hammer system. The bit was missing gauge buttons from the outside of the wings. The casing was shortened to a single joint, and a new wing-style reamer bit was installed. We elected to reenter the short hole started with our previous installation attempt to reduce the required depth of penetration. After a total of ~13 m of penetration, the penetration rate was so slow we decided to release the casing and continue with the reentry funnel deployment. However, we could not extract the pilot bit from the hole even after multiple attempts. After a several-hour struggle, we were finally able to extract the assembly, casing in tow, from the seabed. When brought to the rig floor, we determined the running tool had released the casing, but the wing-style reamer bit was lodged in the lower end of the casing, preventing extraction of the bit. One reamer arm was missing and the lower part of the casing was bent. Since no installation was successful, but basalt pieces were recovered from behind the arms of the hammer and within the casing, we elected to call all the attempts collectively Hole U1310A and curated the material recovered as Core 304-U1310A-1M (miscellaneous).

For fear that the missing reamer arm lay at the bottom of Hole U1310A, the vessel was offset 10 m to the east and an RCB coring assembly was deployed to initiate a bare rock penetration in Hole U1310B. Hole U1310B was spudded at 2250 h on 15 December. The first coring interval (Core 304-U1310B-1R; 0–18.5 mbsf; recovery = 7%) required 30 h to complete. High torque and rubble falling into the hole were relentless during the coring operation. After recovering Core 304-U1310B-1R, 3 m of fill had to be cleared from the hole before continuing coring. Cutting Core 304-U1310B-2R required an additional 16.5 h. When the wireline failed to retrieve the core barrel (after

two attempts), the operations team surmised we had lost the lower part of the BHA. Recovery of the pipe proved this to be the case and ended operations at Site U1310.

Site U1311 (Alternate Site AMHW-02A)

A <1 nmi transit brought us to our alternate hanging wall drilling location. After a brief subsea camera survey, Hole U1311A was spudded with an RCB assembly at 2040 h on 18 December. Core 304-U1311A-1R (0–12 mbsf) required >26 h to cut.

After the first core had been cut in Hole U1311A there was at least 3 m of fill in the 12 m deep hole. We attempted to clear the hole for several hours, without success, and the hole was abandoned. Based on our prespud bottom survey, we elected to move ~100 m north, survey another location, and attempt another hole at this site.

Since we had not been able to keep a hole clear of fill at Site U1310 or in Hole U1311A, we decided to attempt to drill a large-diameter bore without coring. We hoped this strategy would allow deployment of a casing to isolate the upper part of the formation and allow deeper penetration. The two options left in our arsenal of drilling tools were a large rotary bit and the wing-style, reaming hammer bit. We surmised that the rotary bit was not likely to be successful, based on our attempts with rotary coring bits. The larger bit face would translate to less weight on bit per unit area, thus yielding even slower penetration rates. In addition, the size difference between the top of the bit and the BHA would provide ample space for rocks falling into the hole to trap the bit. After a brief subsea camera survey, we chose a location with a smooth sediment cover to deploy the hammer bit. Although there was an initial rapid penetration rate, at a depth of only a few meters below seafloor penetration virtually ceased. High torque stalled rotation, and picking the bit up off bottom to regain rotation allowed rock to cascade into the hole underneath the bit. We hammered for ~19 h, but could gain no headway, so operations at Site U1311 were terminated.

Return to Site U1309 (Proposed Site AMFW-01A)

Following a pipe trip to install an RCB BHA, we reentered Hole U1309D through the HRRS and recommenced coring at 131 mbsf. Cores 304-U1309D-23R to 47R (131.0–252.4 mbsf) were cut, with an average recovery of 64%. We made a pipe trip to pick up a fresh bit, and coring continued through Core 304-U1309D-78R with 74% recovery (average recovery for Hole 1309D = 58%). We terminated coring at 401.3 mbsf after the RCB bit had accumulated 56 rotating hours. The hole was cleaned and filled

with freshwater in preparation for logging. A shallow-penetration hole (Hole U1309E) was cored to 3.8 mbsf 10 m east of Hole U1309D (Core 304-U1309E-1R). Continuing with efforts to capture the oldest sediments draping the central dome of Atlantis Massif, as well as the detachment surface, we moved the vessel in DP mode to a site 275 m northwest of Hole U1309D. Hole U1309F was initiated with the RCB and cored to 4.8 mbsf (Core 304-U1309F-1R). Since RCB coring was not successful in recovering the uppermost basement in either Hole U1309E or U1309F, we tripped the pipe in preparation for logging.

We reentered Hole U1309D with a new APC/XCB bit, and our intention was to log the hole then attempt shallow cores with the XCB. The bit was positioned in the casing, but the logging tools were unable to pass an obstruction at ~40 mbsf. Since the XCB bit would not fit in the RCB hole, we terminated the logging attempt and pursued shallow-penetration coring. We made a transit in DP mode to an alternate location on the dome, where a submersible dive had observed a hard carbonate cap (interpreted to represent the oldest sediment cover on the dome) directly overlying basement. Core 304-U1309G-1X was cored to 3.5 mbsf, but no hard carbonate or recognizable fault rock was recovered. We elected to make a final attempt to recover the lithified carbonate and upper basement with the APC. Only the upper half of the APC barrel returned. Subsequently, we chose to trip the pipe to install a logging bit to guide the pipe past the obstruction in Hole U1309D and accomplish our logging objectives in that hole. Triple-combo and FMS-sonic tool string runs were successful, but an Ultrasonic Borehole Imager (UBI) run was not attempted since the second FMS pass ended with fallen rock briefly trapping the tool in the hole. The tool was extracted with no significant damage.

After logging operations were concluded, there was sufficient time left in the expedition for a short bit run. We elected to attempt a single, short RCB core at the same location as Hole U1309G. Using the retired bit from our last coring run, we attempted coring to a depth of just more than 2 m below the soft sediment blanket, but the core barrel returned empty. With ~5 h of operations time left in the expedition, the bit was returned to the seafloor and Core 304-U1309H-1R was cut without circulation in the upper 0.5 m and low pump pressure for the remainder of coring (~3.5 m). The pipe was pulled and inspected, and we were under way for Ponta Delgada by 0700 h on 4 January 2005.

REFERENCES

Agar, S.M., and Lloyd, G.E., 1997. Deformation of Fe-Ti oxides in gabbroic shear zones from the MARK area. In Karson, J.A., Cannat, M., Miller, D.J., and Elthon, D. (Eds.), *Proc. ODP, Sci. Results,* 153: College Station, TX (Ocean Drilling Program), 123–141.

Blackman, D.K., Cann, J.R., Janssen, B., and Smith, D.K., 1998. Origin of extensional core complexes: evidence from the MAR at Atlantis fracture zone. *J. Geophys. Res.,* 103:21315–21334.

Blackman, D.K., Karson, J.A., Kelley, D.S., Cann, J.R., Früh-Green, G.L., Gee, J.S., Hurst, S.D., John, B.E., Morgan, J., Nooner, S.L., Ross, D.K., Schroeder, T.J., and Williams, E.A., 2004. Geology of the Atlantis Massif (MAR 30°N): implications for the evolution of an ultramafic oceanic core complex. *Mar. Geophys. Res.,* 23:443–469.

Buck, W.R., 1988. Flexural rotation of normal faults. *Tectonics,* 7:959–973.

Canales, J.P., Tucholke, B.E., and Collins, J.A., 2004. Seismic reflection imaging of an oceanic detachment fault: Atlantis megamullion (Mid-Atlantic Ridge, 30°10′N). *Earth Planet. Sci. Lett.,* 222:543–560.

Cann, J., Blackman, D., Morgan, J., and *MARVEL* cruise participants, 2001. Geological inferences about the Mid-Atlantic Ridge 30°N core complex from initial analysis of side-scan, bathymetry and basalt petrography. *Eos, Trans. Am. Geophys. Union,* 82:F1099.

Cann, J.R., Blackman, D.K., Smith, D.K., McAllister, E., Janssen, B., Mello, S., Avgerinos, E., Pascoe, A.R., and Escartin, J., 1997. Corrugated slip surfaces formed at ridge-transform intersections on the Mid-Atlantic Ridge. *Nature,* 385:329–332.

Cannat, M., Bideau, D., and Bougault, H., 1992. Serpentinized peridotites and gabbros in the Mid-Atlantic Ridge axial valley at 15°37′N and 16°52′N. *Earth Planet. Sci. Lett.,* 109:87–106.

Casey, J.F., 1997. Comparison of major- and trace-element geochemistry of abyssal peridotites and mafic plutonic rocks with basalts from the MARK region of the Mid-Atlantic Ridge. In Karson, J.A., Cannat, M., Miller, D.J., and Elthon, D. (Eds.), *Proc. ODP, Sci. Results,* 153: College Station, TX (Ocean Drilling Program), 181–241.

Collins, J.A., Tucholke, B.E., and Canales, J.-P., 2001. Structure of Mid-Atlantic Ridge megamullions from seismic refraction experiments and multichannel seismic reflection profiling. *Eos, Trans. Am. Geophys. Union,* 82:F1100. (Abstract)

Detrick, R.S., and Collins, J.A., 1998. Seismic structure of ultramafics exposed at shallow crustal levels in the Mid-Atlantic Ridge rift valley at 15°N. *Eos, Trans. Am. Geophys. Union,* 79:F800. (Abstract)

Dick, H.J.B., Natland, J.H., Miller, D.J., et al., 1999. *Proc. ODP, Init. Repts.,* 176 [CD-ROM]. Available from: Ocean Drilling Program, Texas A&M University, College Station, TX 77845-9547, U.S.A.

Escartin, J., Mével, C., MacLeod, C.J., and McCaig, A., 2003. Constraints on deformation conditions and the origin of oceanic detachments, the Mid-Atlantic Ridge core complex at 15°45′N. *Geochem., Geophys., Geosyst.,* 4:10.1029/2002GC000472.

Früh-Green, G.L., Kelley, D.S., Bernasconie, S.M., Karson, J.A., Ludwig, K.A., Butterfield, D.A., Boschi, C., and Proskurowksi, G., 2003. 30,000 years of hydrothermal activity at the Lost City vent field. *Science,* 301:495–498.

Früh-Green, G., Kelley, D.S., Karson, J.A., Blackman, D.K., Boschi, C., John, B.E., Schroeder, T., Ross, D.K., and *MARVEL* cruise participants, 2001. Hydrothermal alteration, serpentinization and carbonate precipitation at the Lost City vent field (30°N MAR). *Eos, Trans. Am. Geophys. Union,* 82:F1101.

John, B.E., 1987. Geometry and evolution of a mid-crustal extensional fault system: Chemehuevi Mountains, southeastern California. In Coward, M.P., Dewey, J.F., and Hancock, P.L. (Eds.), *Continental Extensional Tectonics,* Spec. Publ.—Geol. Soc. Am., 28:313–335.

Karson, J.A., 2003. Unconformities in slow-spread oceanic crust: implications for spreading processes and dismembered ophiolites, *Eos, Trans. Am. Geophys. Union,* 84:F1506. (Abstract)

Kelemen, P.B., Kikawa, E., Miller, D.J., et al., 2004. *Proc. ODP, Init. Repts.,* 209 [CD-ROM]. Available from: Ocean Drilling Program, Texas A&M University, College Station TX 77845-9547, USA.

Kelley, D.S., Karson, J.A., Blackman, D.K., Früh-Green, G.L., Butterfield, D.A., Lilley, M.D., Olson, E.J., Schrenk, M.O., Roe, K.K., Lebon, G.T., and Rivizzigno, P., 2001. An off-axis hydrothermal vent field near the Mid-Atlantic Ridge at 30°N. *Nature (London, U. K.),* 412(6843):145–149.

Kelley, D.S., Karson, J.A., Yoerger, D., Früh-Green, G.L., Butterfield, D.A., and Lilley, M., 2003. Discovering new mantle-hosted submarine ecosystems: the Lost City hydrothermal field. Eos, *Trans. Am. Geophys. Union,* 84:F230.

Lavier, L., Buck, W.R., and Poliakov, A.N.B., 1999. Self-consistent rolling-hinge model for the evolution of large-offset low-angle normal faults. *Geology,* 27:1127–1130.

MacLeod, C.J., Escartin, J., Banerji, D., Banks, G.J., Gleeson, M., Irving, D.H.B., Lilly, R.M., McCaig, A.M., Niu, Y., Allerton, S., and Smith, D.K., 2002. Direct geological evidence for oceanic detachment faulting: the Mid-Atlantic Ridge, 15°45′N. *Geology,* 30:10:879–882.

Miller, M.G., 1996. Ductility in fault gouge from a normal fault system, Death Valley, California: a mechanism for strengthening and relevance to paleoseismicity. *Geology,* 24:603–606.

Nooner, S.L., Sasagawa, G.S., Blackman, D.K., and Zumberge, M.A., 2003. Constraints on crustal structure at the Mid-Atlantic Ridge from seafloor gravity measurements made at the Atlantis Massif. *Geophys. Res. Lett.,* 30:10.1029/2003GL017126.

Schroeder, T., and John, B.E., 2004. Strain localization on an oceanic detachment fault system, Atlantis Massif, 30°N, Mid-Atlantic Ridge. *Geochem., Geophys., Geosyst.,* 5:10.1029/2004GC000728.

Schroeder, T., John, B.E., Kelley, D., and *MARVEL* cruise participants, 2001. Microstructural observations of an "oceanic core complex": Atlantis Massif, 30°N Mid-Atlantic Ridge. *Eos, Trans. Am. Geophys. Union,* 82:F1100.

Spencer, J.E., 1985. Miocene low-angle normal faulting and dike emplacement, Homer Mountain and surrounding areas, southeastern California and southernmost Nevada. *Geol. Soc. Am. Bull.,* 96:110–1155.

Vening Meinesz, F.A., 1950. Les graben Africains resultant de compression oe de tension dans la croute terrestres? *Kol. Inst. Bull.,* 21:539–552.

Wernicke, B.P., and Axen, G.J., 1988. On the role of isostasy in the evolution of normal fault systems. *Geology,* 16:848–451.

Table T1. Expedition 304 site summaries.

Hole	Latitude	Longitude	Seafloor depth (mbrf)	Cores (*N*)	Cored (m)	Recovered (m)	Recovery (%)	Drilled (m)	Total penetration (m)	Time on hole (h)	Time on hole (days)
U1309A	30°10.1081′N	42°7.1101′W	1653.4	1	2.0	1.92	96.0	0.0	2.0	14.75	0.6
U1309B	30°10.1081′N	42°7.1101′W	1653.4	20	101.8	46.70	45.9	0.0	101.8	152.83	6.4
U1309C	30°10.1081′N	42°7.1209′W	1646.0	0	0.0	0.00	0.0	6.0	6.0	47.83	2.0
U1309D	30°10.1195′N	42°7.1131′W	1656.0	78	380.8	243.81	64.0	20.5	401.3	431.08	18.0
U1309E	30°10.1207′N	42°7.1057′W	1656.0	1	3.8	5.6	147.4	0.0	3.8	3.25	0.1
U1309F	30°10.1999′N	42°7.2518′W	1656.0	1	4.8	6.1	126.9	0.0	4.8	14.58	0.6
U1309G	30°10.5379′N	42°6.3179′W	1885.0	1	4.8	6.1	126.9	0.0	4.8	16.92	0.7
U1309H	30°10.5379′N	42°6.3179′W	1885.0	1	4.0	0.2	4.8	0.0	4.0	23.4	1.0
		Site U1309 totals:		103	502.0	310.40	61.8	26.5	528.5	704.67	29.4
U1310A	30°11.4850′N	42°3.9256′W	2594.0	0	0.00	0.00	NA	12.0	12.0	115.42	4.8
U1310B	30°11.4842′N	42°3.9197′W	2594.0	2	23.0	1.30	5.7	0.0	23.0	66.67	2.8
U1311A	30°10.6091′N	42°4.1904′W	2552.0	2	12.0	1.71	14.3	0.0	12.0	57.33	2.4
U1311B	30°10.6595′N	42°4.2170′W	2516.0	0	0.0	0.00	0.0	10.6	10.6	37.42	1.6
		Site U1310 and U1311 totals:		4	35	3.0	8.6	22.6	57.6	276.8	11.5
		Expedition 304 totals:		107	537.0	313.41	58.4	49.1	586.1	981.50	40.9

Figure F1. Tectonic and morphologic setting of Atlantis Massif. Bathymetric contours illustrate the deep median valley of the Mid-Atlantic Ridge and its intersection with the Atlantis transform fault. The shallow dome comprising the core of Atlantis massif has two structural components: the central dome, where IODP footwall work was focused, and the southern ridge. The eastern volcanic block contains the hanging wall IODP sites.

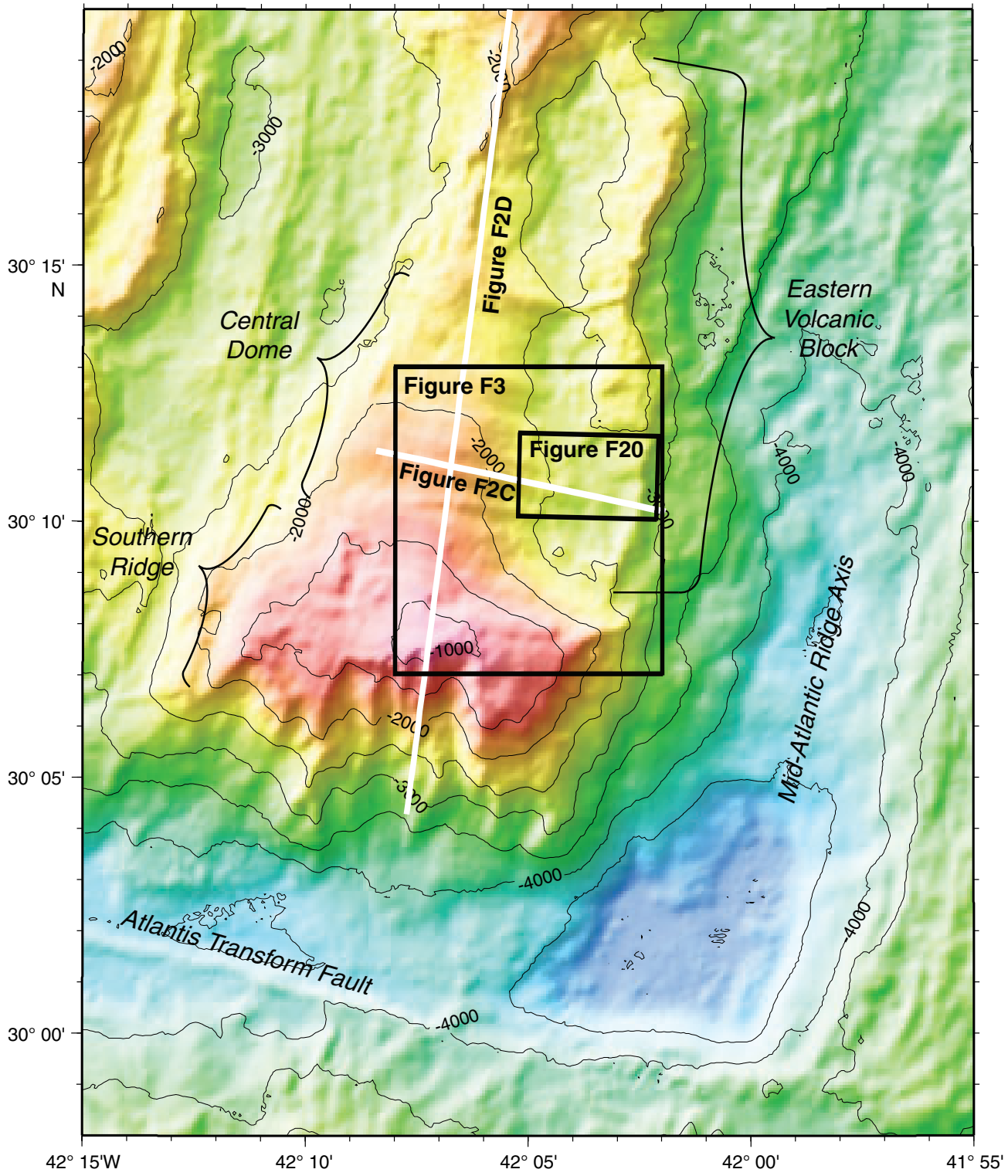

Figure F2. Seismic profiles indicate the subsurface structure of the central dome and eastern block of Atlantis Massif. **A.** Deep source refraction (NOBEL Line 9) recorded by an ocean bottom hydrophone shows high velocity arrivals (8 km/s) at very short range. **B.** Velocity gradient at Atlantis Massif; gradient is similar to that determined near Ocean Drilling Program (ODP) Hole 920, where serpentinized peridotite was recovered. The gradient near Hole 735B, where only gabbro has been recovered, is not as great. MARK = Mid-Atlantic Ridge south of the Kane Fracture Zone, MAR = Mid-Atlantic Ridge, SWIR = Southwest Indian Ridge. **C.** A portion of Multichannel seismic (MCS) Line Meg10 across the Central Dome. **D.** MCS Line Meg4, along the strike of Atlantis Massif. MCS data were collected by the *Ewing* (EW-0102) in 2001 using a 10-gun array with 3100 in^3 (51 L) capacity. Shot spacing was 37.5 m. Canales et al. (2004) processed the data by common midpoint (CMP) gathers, deconvolution, normal moveout correction, dip moveout correction, and stacking. In addition, record section in D has been time migrated. (**Figure shown on next page.**)

Figure F2. Caption shown on previous page.

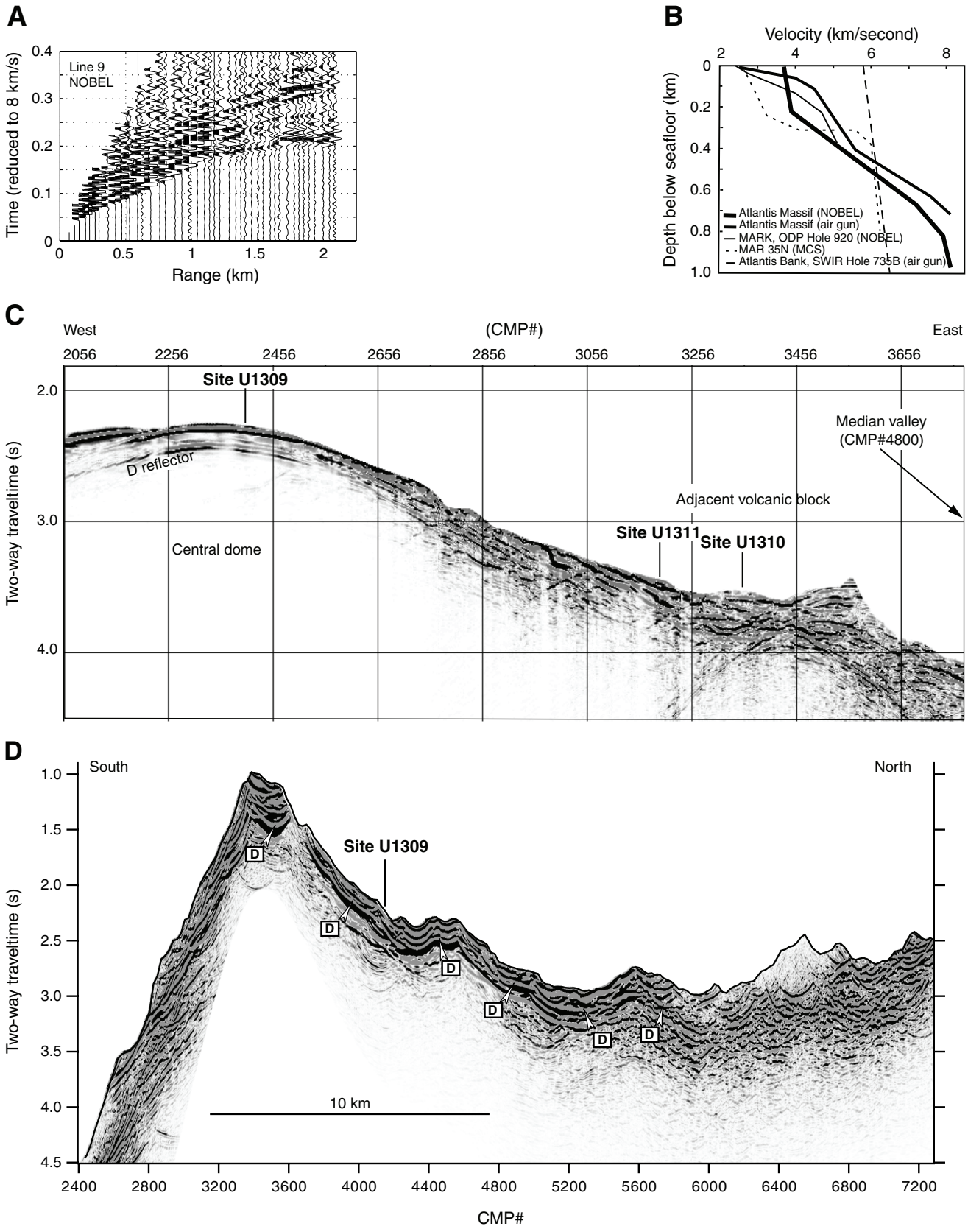

Figure F3. Basemap of Atlantis Massif showing prior geological and geophysical data coverage and the location of IODP drill sites (circles). Bathymetry is contoured at 20 m intervals, based on a 100 m grid. Seismic reflection and refraction lines and seafloor mapping/sampling sites are shown. Spreading-parallel multichannel seismic (MCS) Line Meg-9 follows the southern ridge; Meg-10 crosses the central dome. Line Meg-5 crosses the southeast shoulder of the massif and then subparallels the trend of the adjacent volcanic block. The corrugated detachment surface capping the central dome is inferred to extend beneath this eastern block, thereby making the upper crustal volcanics a hanging wall to the fault. MCS = multichannel seismic, CMP = common midpoint.

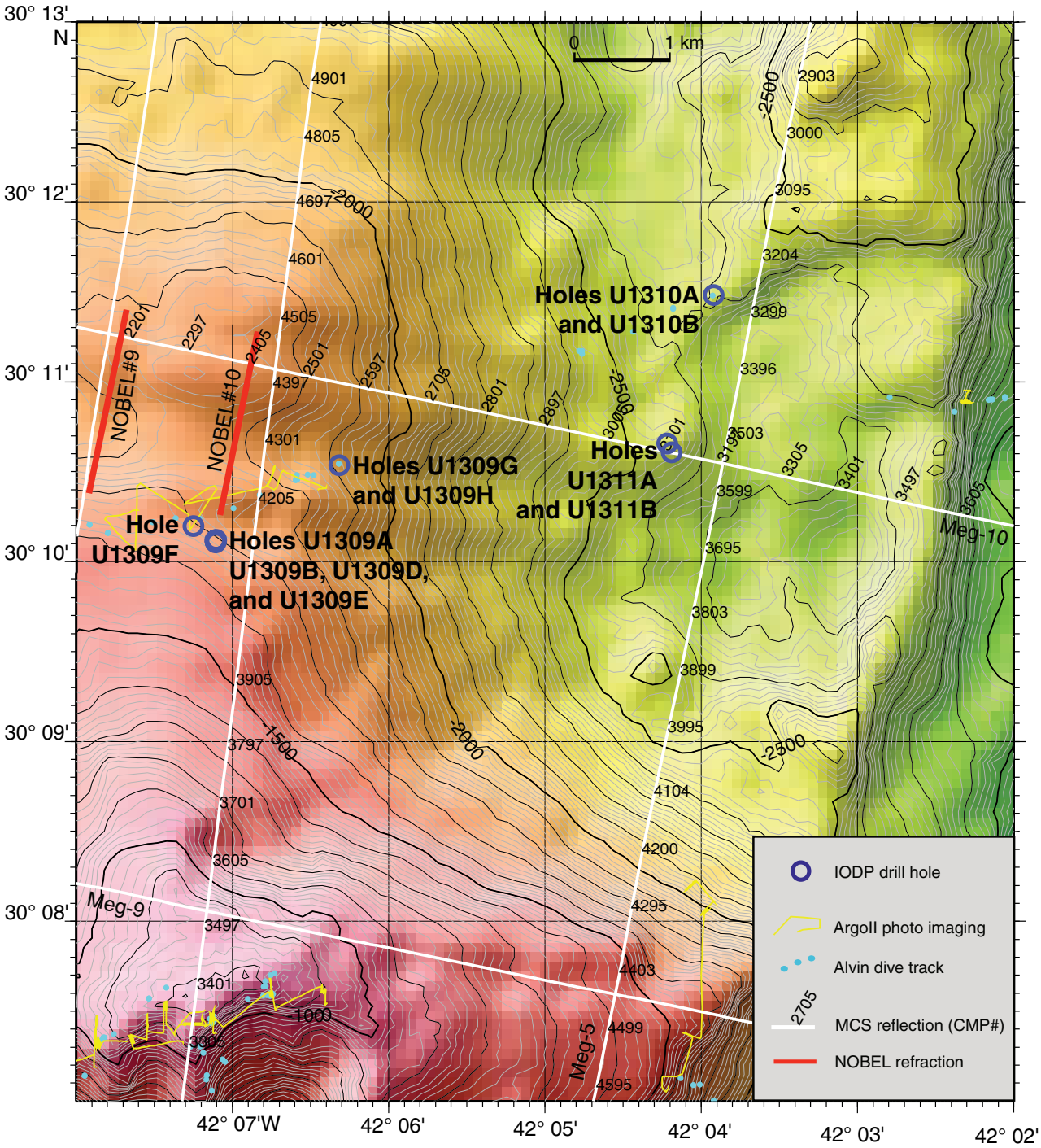

Figure F4. Core scan of recovered basalt, talc-tremolite schist, and fractured diabase from Hole U1309H.

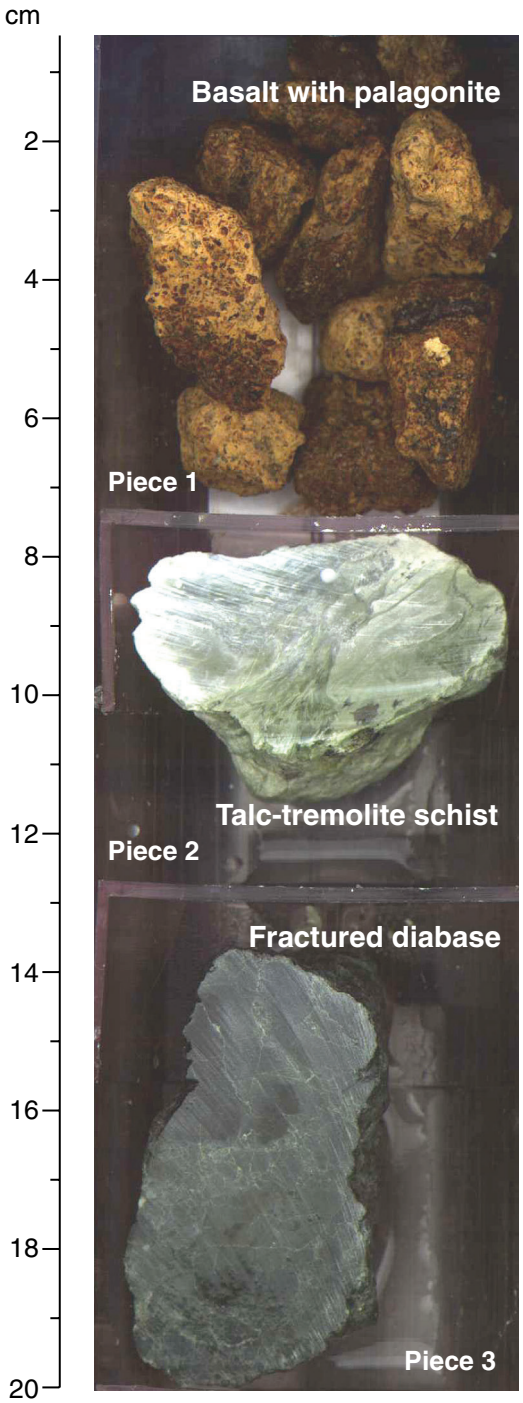

Figure F5. Lithologic columns for Holes U1309B (left) and U1309D (right 4). The individual units are grouped into Gabbroic zones (1–10; labeled to the right of each lithology column) that display similar dominant rock type and/or presence of intercumulus phases. Core numbers are shown on the left of each lithology column.

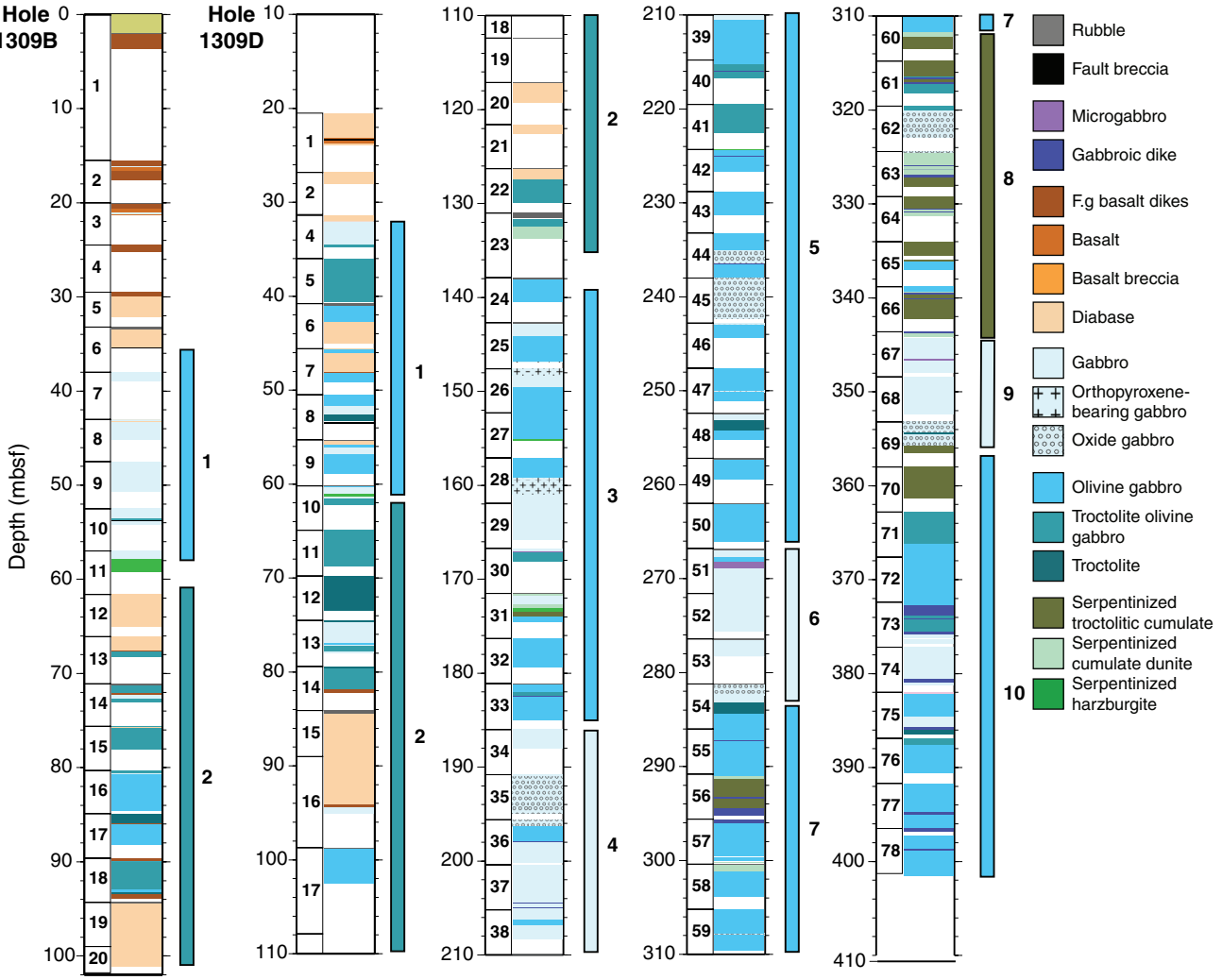

Figure F6. Lithologic summary for Holes U1309B and U1309D.

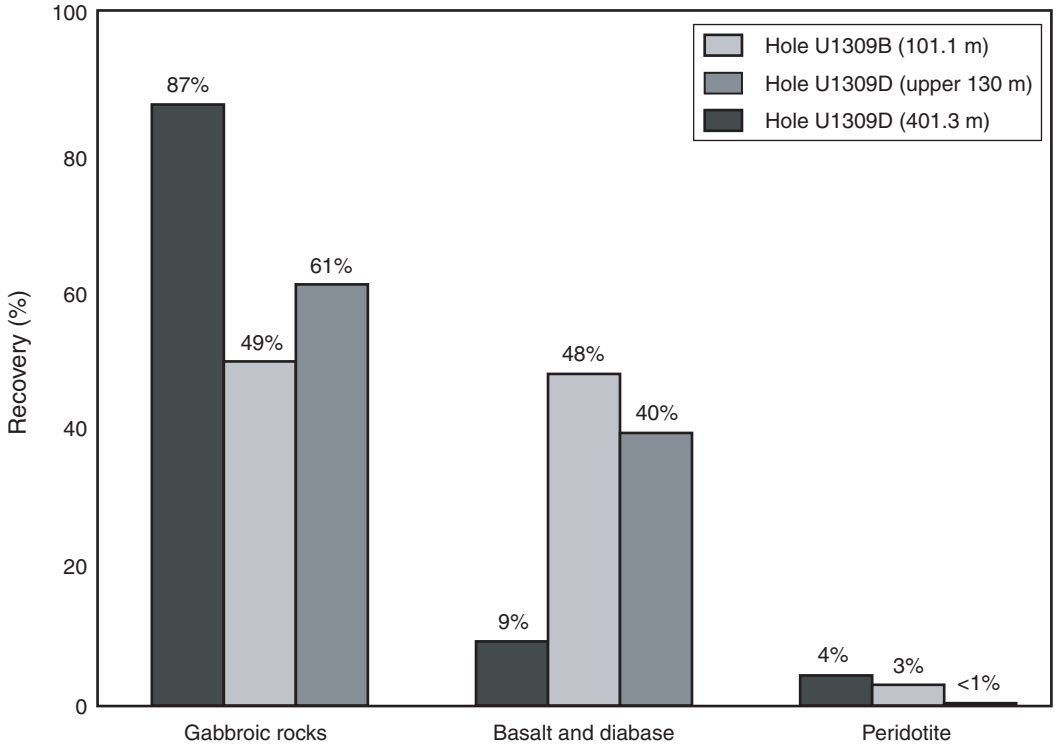

Figure F7. Igneous contact in Hole U1309B. Note the sharp contact, downward increase in grain size over the 10 cm interval below the contact, and upward increase in size and abundance of plagioclase phenocrysts.

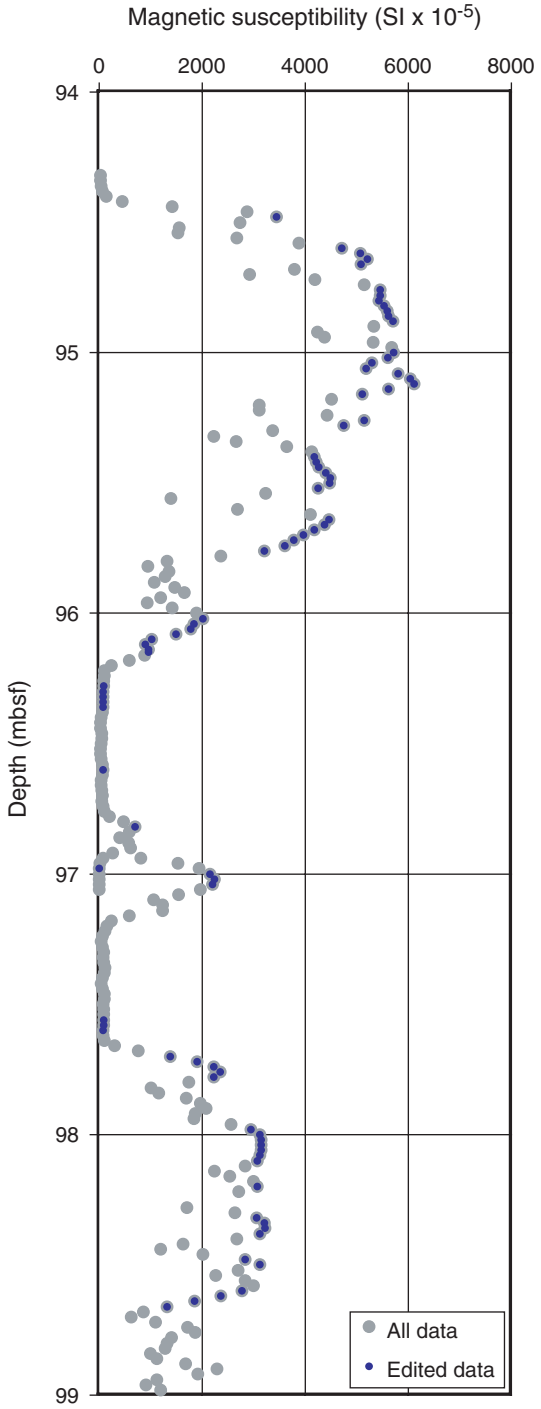

Figure F8. MST magnetic susceptibility between 94 and 99 mbsf in Hole U1309B.

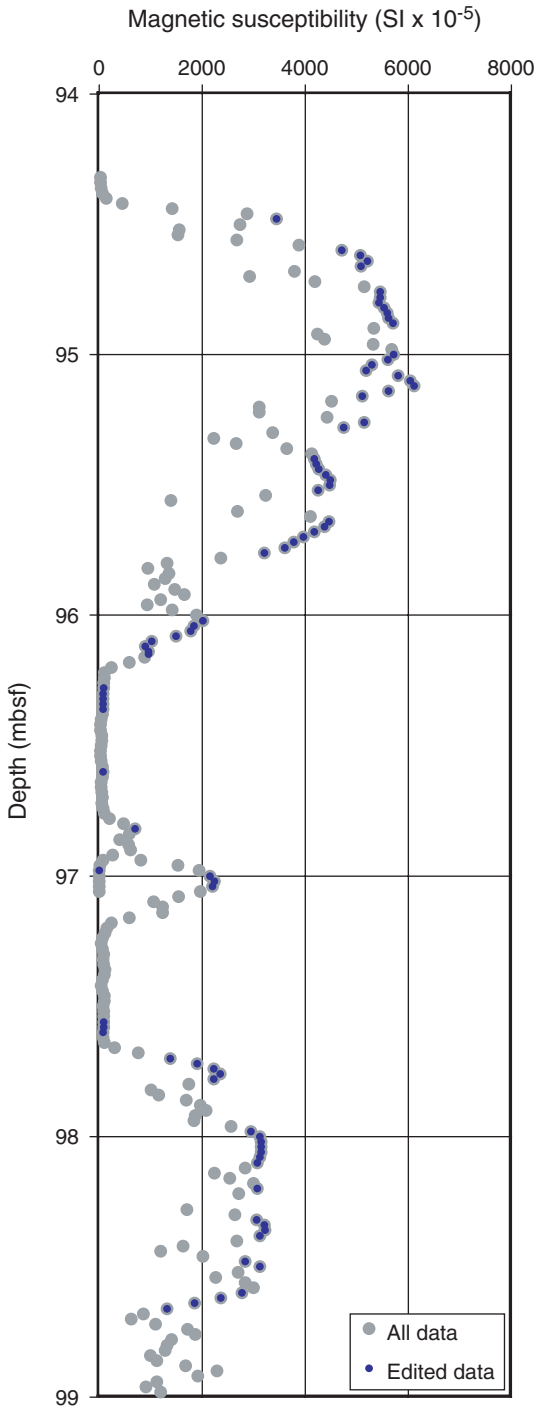

Figure F9. Volatile free (**A**) SiO_2, (**B**) CaO, (**C**) Al_2O_3, (**D**) Na_2O, (**E**) Fe_2O_3, and (**F**) TiO_2 contents versus MgO content for basalts, diabases, and basalt breccia from Site U1309. MAR = Mid-Atlantic Ridge.

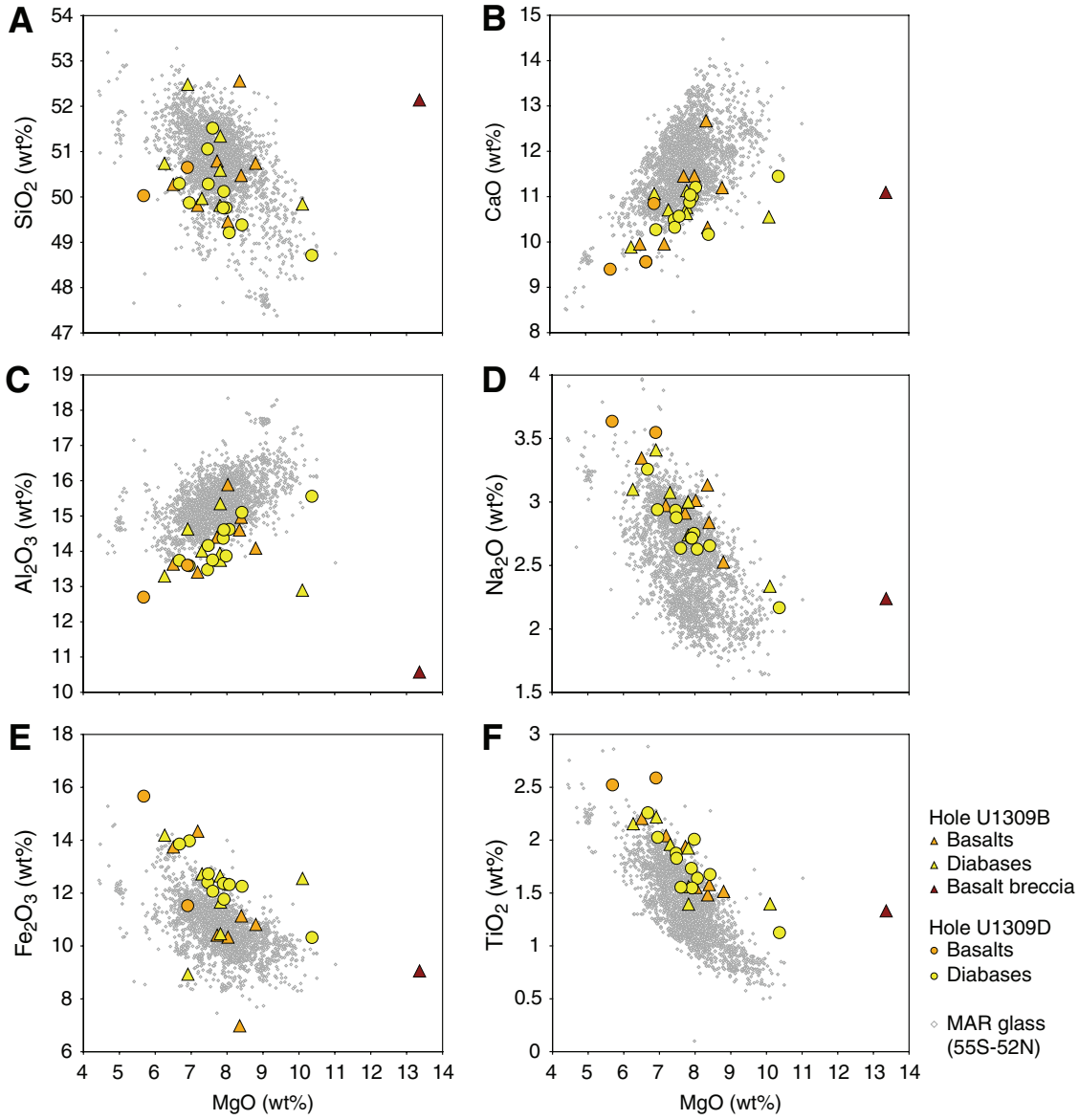

Figure F10. Termination of a late magmatic leucocratic vein in Core 304-U1309D-62R.

Figure F11. Volatile free (**A**) MgO, (**B**) CaO, (**C**) Fe_2O_3, (**D**) Na_2O, (**E**) Al_2O_3, and (**F**) TiO_2 contents versus SiO_2 content for gabbros and olivine gabbros from Hole U1309B and gabbros, olivine gabbros, troctolites, orthopyroxene-bearing gabbros, oxide gabbros, wehrlite and peridotites from Hole U1309D. The composition of Site U1309 basalts and diabases (beige diamonds) together with a compilation of Mid-Atlantic Ridge (MAR) volcanic glass compositions (open diamonds) downloaded from PetDB in December 2004 (online at **beta.www.petdb.org**) are shown for comparison. Also shown for comparison are published data for Leg 153 gabbros (Agar et al., 1997), Hole 735B (Dick, Natland, Miller, et al., 1999), and Leg 209 gabbros (Kelemen, Kikawa, Miller, et al., 2004).

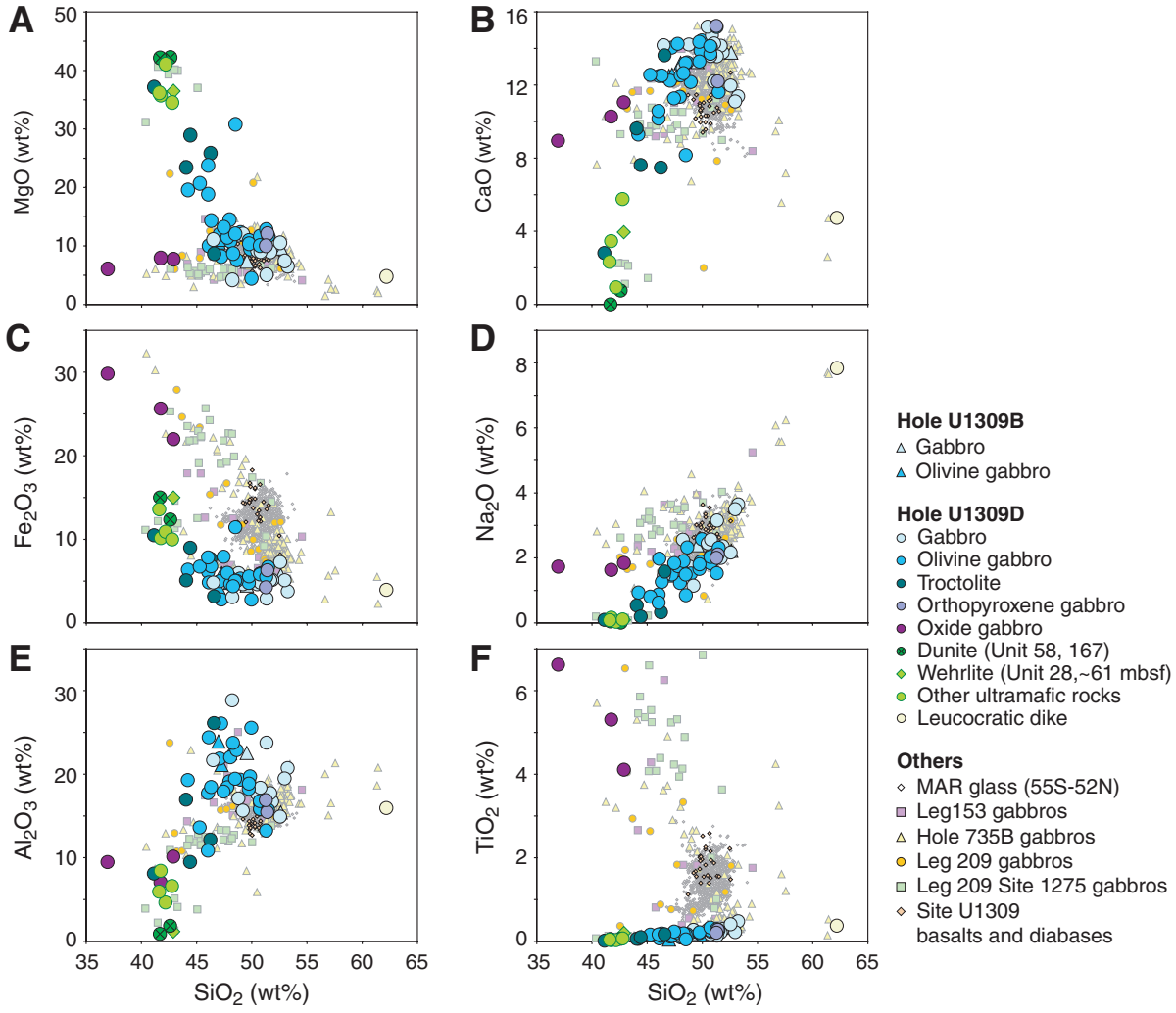

Figure F12. Close-up photographs of (**A**) ultramafic rock with cumulate or melt percolation texture and (**B**) residual mantle peridotite.

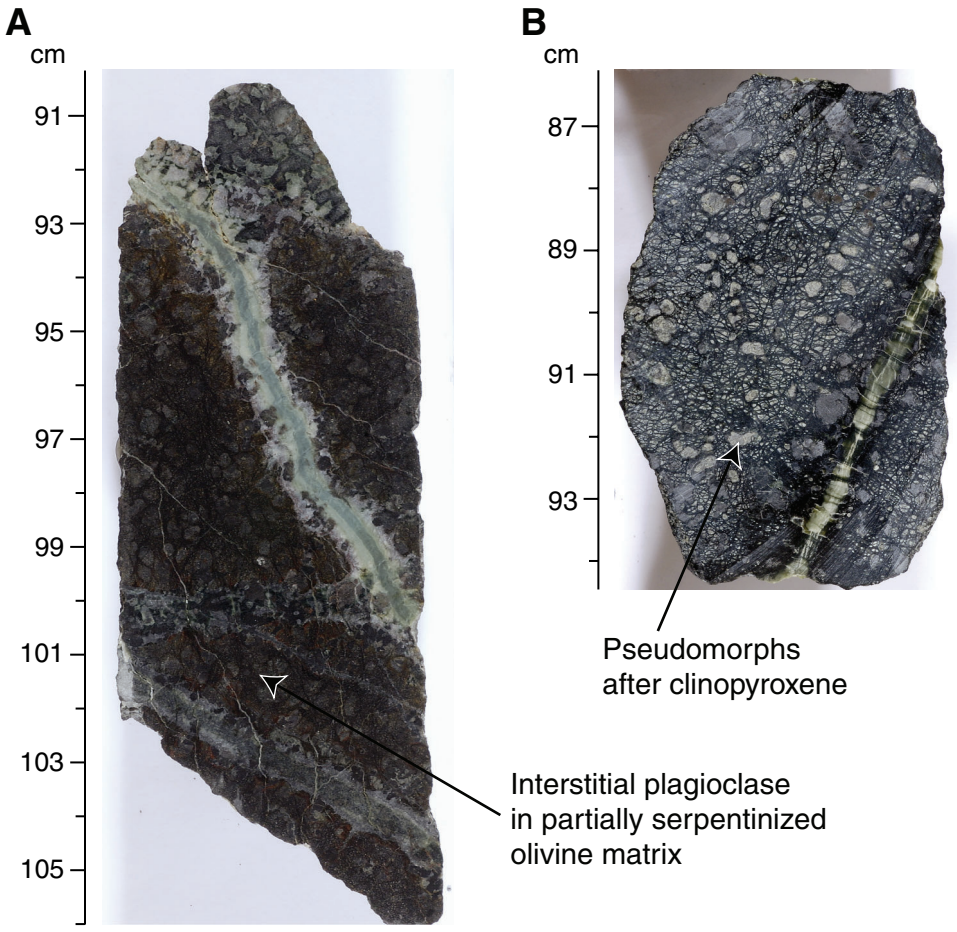

Figure F13. Variation in alteration intensity with depth in Hole 1309D. **A.** Overall degree of alteration in the recovered rock. The red line is alteration intensity averaged over a 5 m interval (normalized to cored intervals only) **B.** Vein-related alteration and brecciation. The red line is average vein-related alteration calculated on a 5 m interval basis (normalized to cored intervals only).

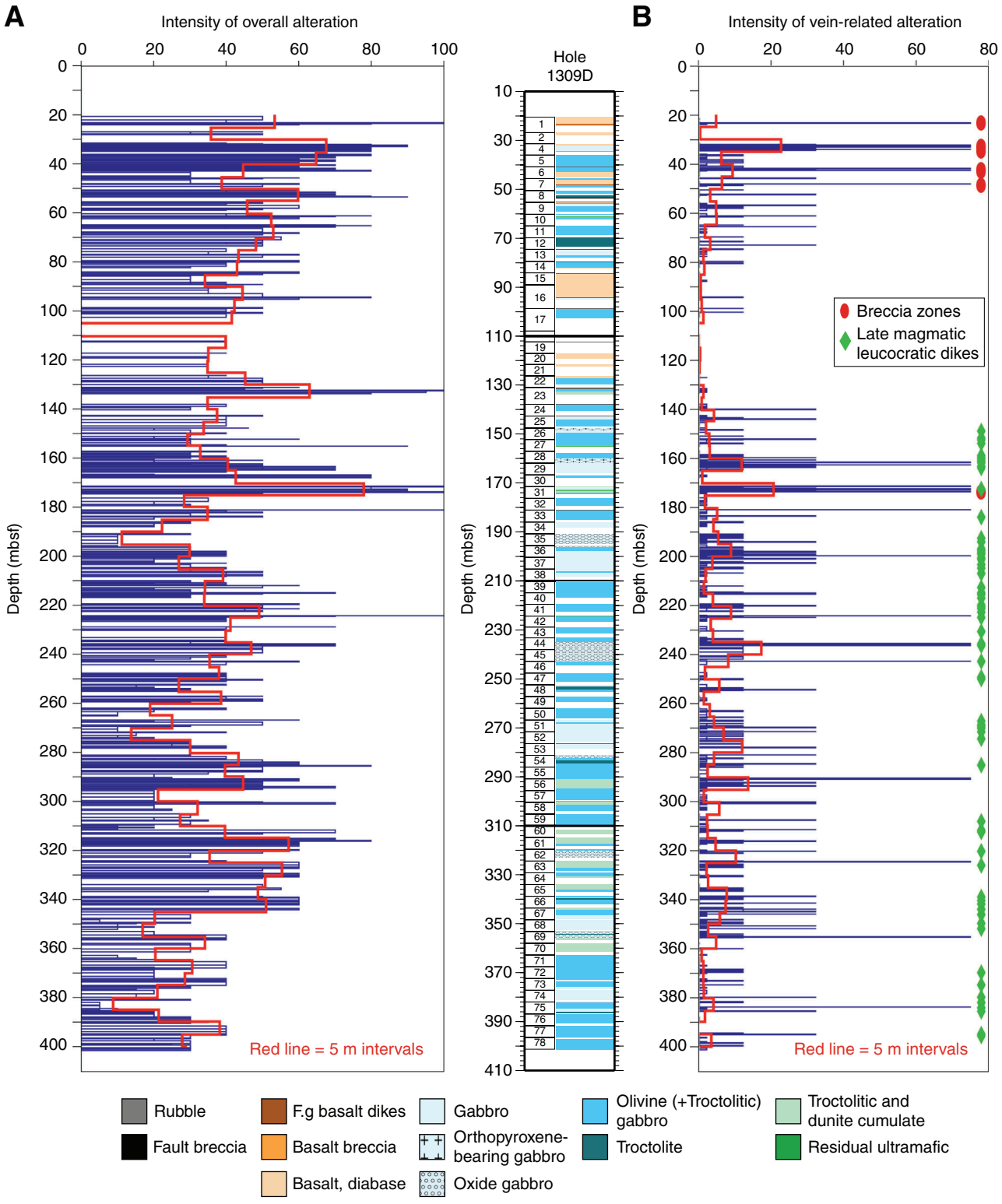

Figure F14. Troctolite layer showing well-developed corona mesh texture. Lighter green areas are actinolite after relict clinopyroxene. Original grain boundaries are outlined by dark green (appears black) chlorite (interval 304-U1309B-15R-2, 53–64 cm).

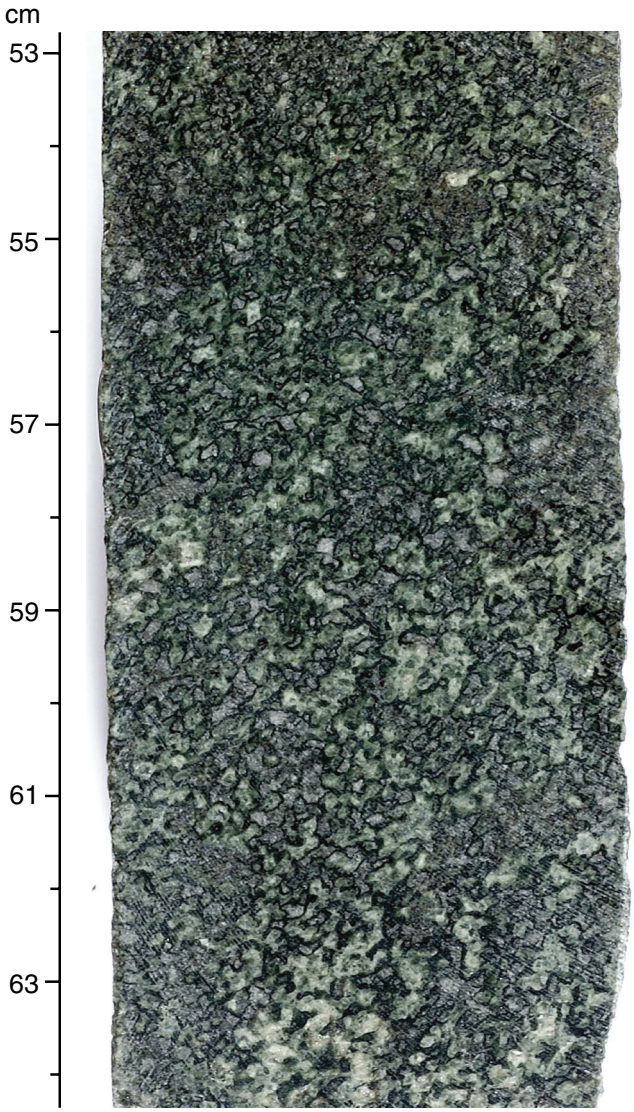

Figure F15. Contact between coarse-grained gabbro and harzburgite in Section 304-U1309B-11R-1. Note the talc-tremolite band between the two lithologies and the variations in serpentinization style.

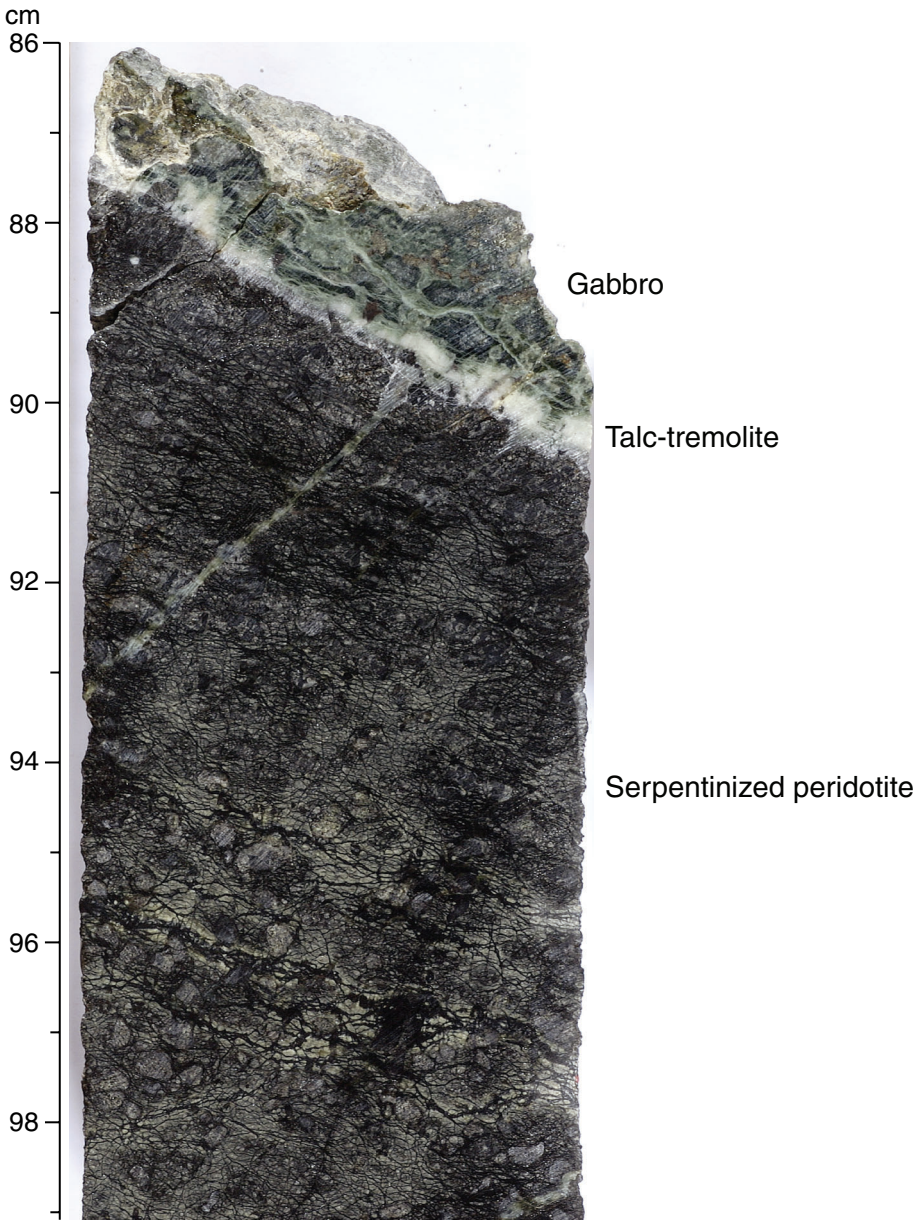

Figure F16. Summary of deformation structures observed on cores from Hole U1309D and in comparison to paleomagnetic data and downhole logging measurements. **A.** Lithologic column. **B.** Intensity of magmatic fabric (3 = strong shape preferred orientation). **C.** Intensity of crystal-plastic fabric (4–5 = mylonitic-ultramylonitc). **D.** Frequency of alteration veins (5 = >20/cm). **E.** Intensity of cataclastic fabric (5 = cataclasite). **F.** Magnetic inclination deduced from core samples that have been demagnetized to remove drilling overprint. Downhole logging results: **G.** Estimate of likelihood that an interval is a fault zone, based on interpretation of Formation Micro Scanner resistivity images. **H.** Caliper data show deviation of borehole diameter from 10 inch reference (0 in plot corresponds to a perfectly gauge hole). **I.** Neutron porosity measurement illustrates relative changes in wall rock porosity. Absolute value is not meaningful here because calibration is for limestone. **J.** Downhole density variation. **K.** Resistivity measured by the Dual Laterolog on the Triple Combo tool. (**Figure shown on next page.**)

Figure F16. Caption shown on previous page.

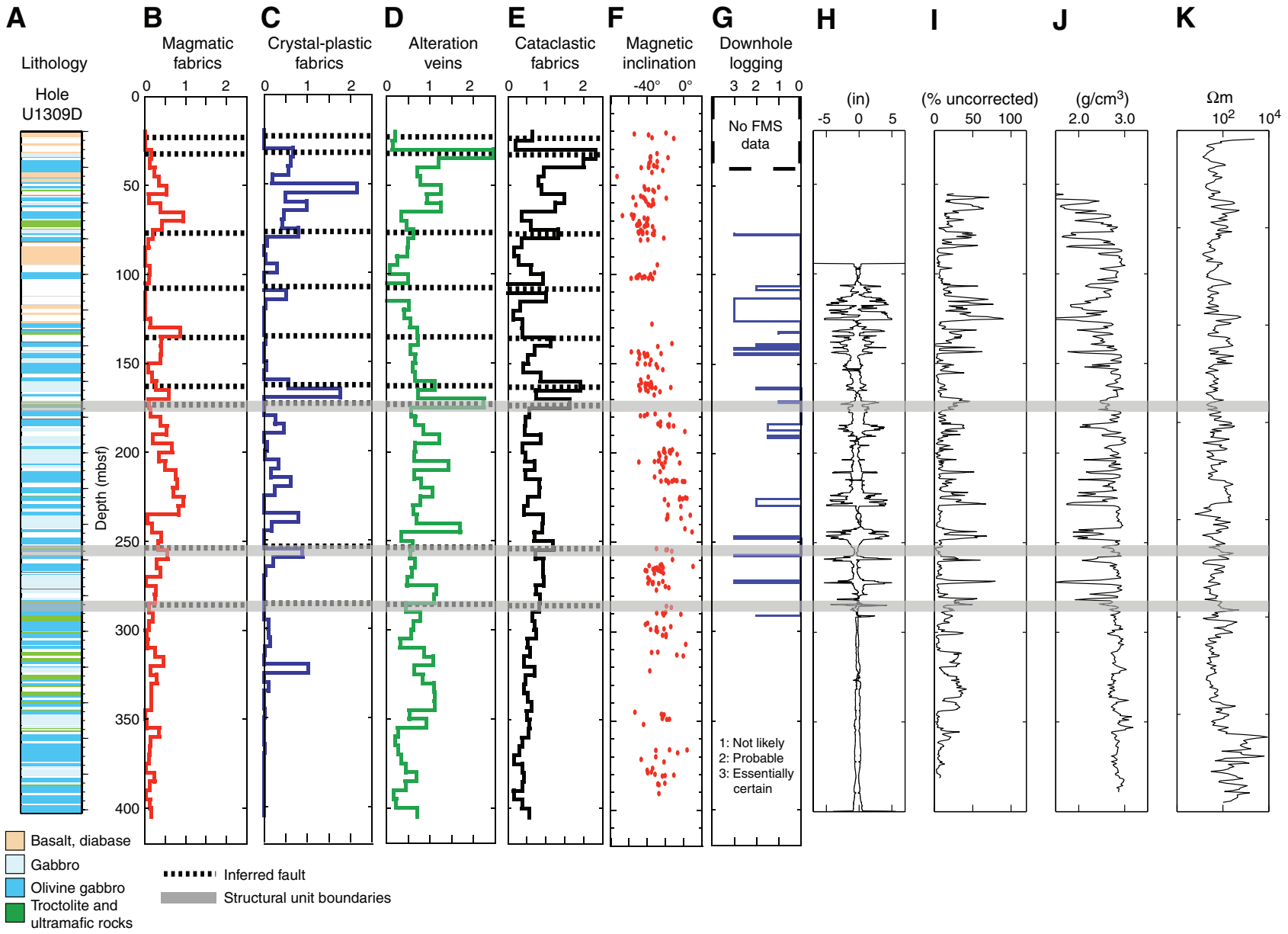

Figure F17. Magmatic layering in gabbro. Olivine gabbro to the right is richer in plagioclase than the troctolite layer on the left, which is characterized by green altered olivine with dark green (black) chlorite rims.

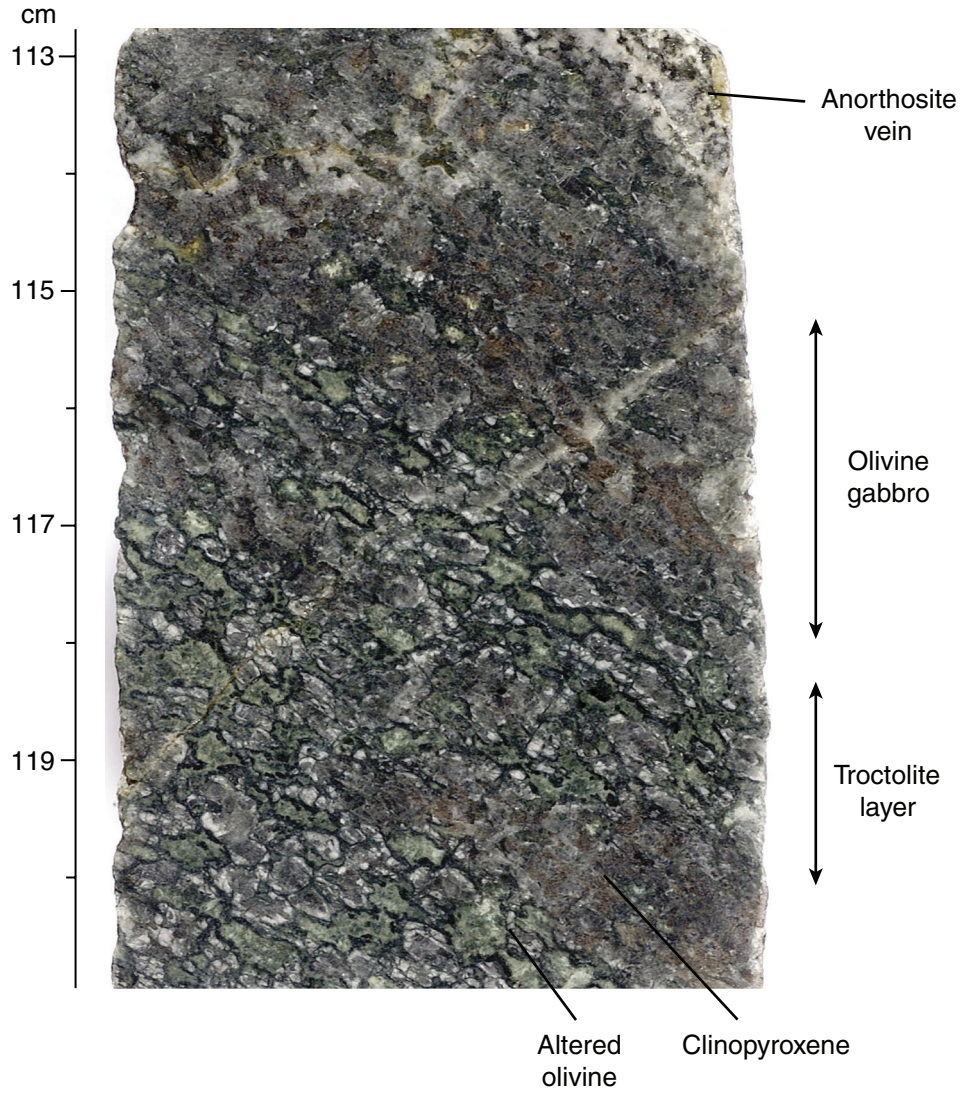

Figure F18. Examples of deformation structure that is recorded in some Hole U1309D rocks. **A.** Whole thin section of Sample 304-U1309D-8R-1, 68–71 cm, showing a well-defined mylonite in gabbro cut by a fracture. **B.** Brown amphibole vein crosscuts highly localized shear zone in a mylonite with domains of recrystallized plagioclase and pyroxene (Sample 304-U1309D-9R-1, 71–73 cm) (field of view = 4 mm).

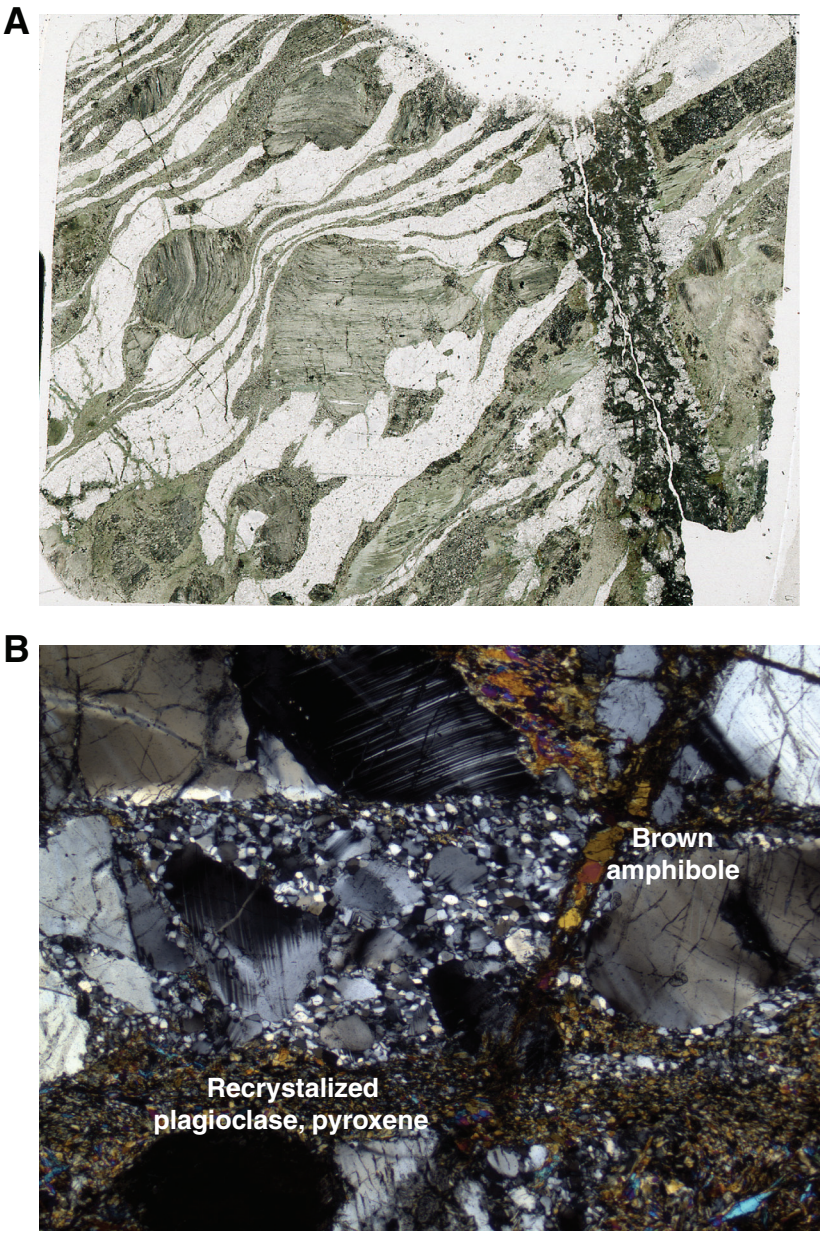

Figure F19. Summary of characteristic remanence inclination from discrete samples from Holes U1309B and U1309D. Insets show inclination distributions in three depth intervals.

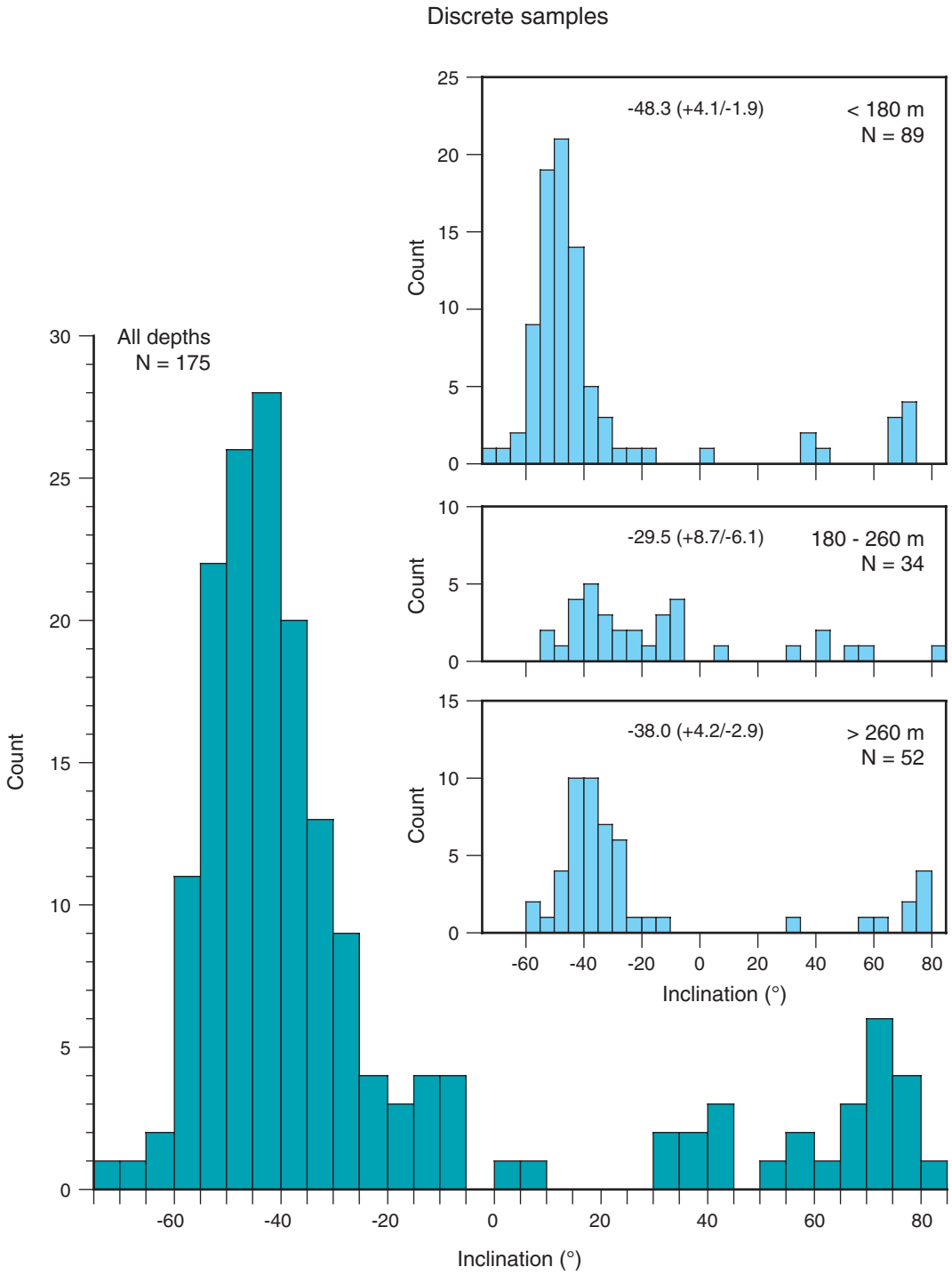

Figure F20. Setting of hanging wall sites. The area shown is 5 km × 3 km; each gridbox = 500 m. Universal Transverse Mercator (UTM) Zone 23 and latitude/longitude coordinates are labeled. Side-scan sonar data are overlain by bathymetric contours (50 m interval), which show the eastern scarp of the hanging wall that drops steeply into the median valley, the relatively gentle topography on the top of the block, and the place where the break in slope from the lower central dome occurs. Sites U1310 and U1311 are both near this inferred contact between the footwall and hanging wall. The side-scan data show several high backscatter features (white) that mark scarps. Several small volcanic mounds can also be recognized from high reflectivity on one side and a small shadow on the other side.

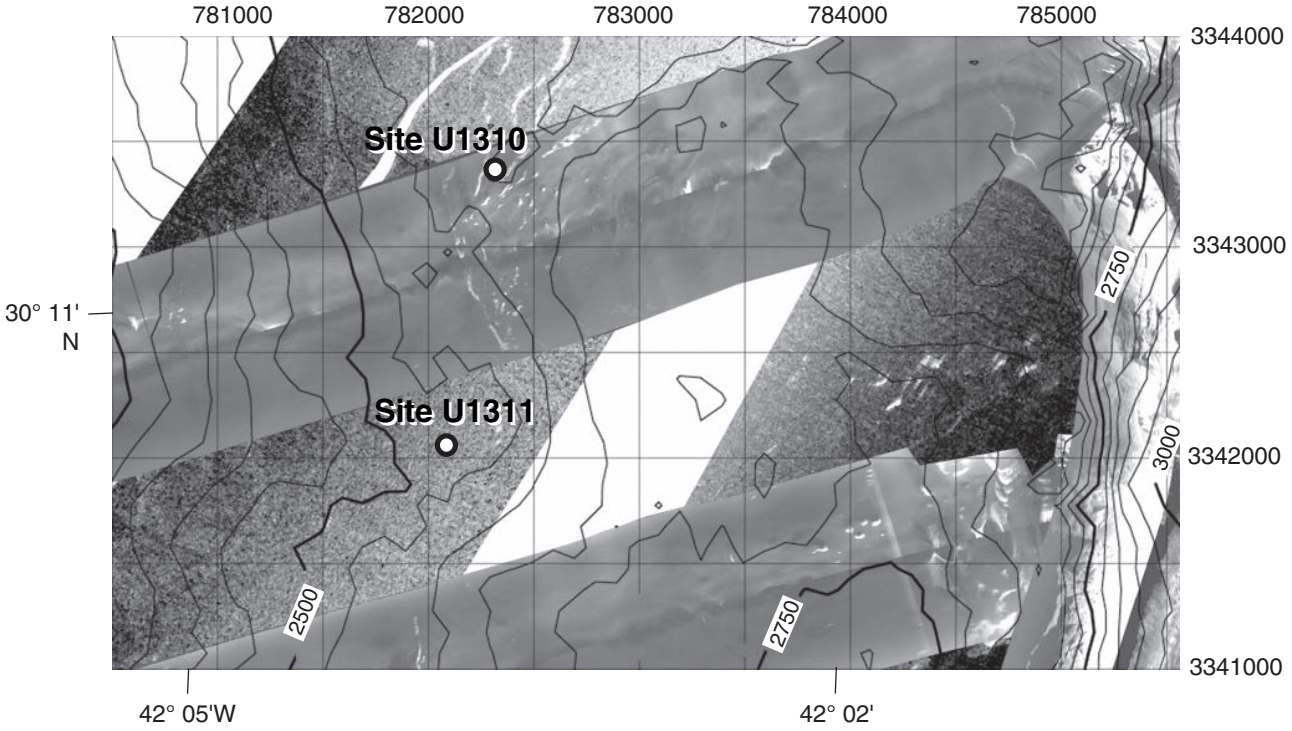

Figure F21. Full thin section scan of basalt from Hole U1311A.